USGS
science for a changing world

Temporal, Spatial, and Chemical Evolution of Quaternary High-Silica Rhyolites in the Mineral Mountains, Utah

Chapter K of
Distributed Volcanism—Characteristics, Processes, and Hazards

Professional Paper 1890

U.S. Department of the Interior
U.S. Geological Survey

Cover. Photograph looking east into the Mineral Mountains, Utah, featuring Quaternary rhyolites, such as the rhyolite of South Twin Flat Mountain (left) above a pumice quarry (white horizontal layer) and Miocene granite (right). Photograph by Tiffany Rivera.

Temporal, Spatial, and Chemical Evolution of Quaternary High-Silica Rhyolites in the Mineral Mountains, Utah

By Tiffany A. Rivera, Brian R. Jicha, Stefan Kirby, and Hannah B. Peacock

Chapter K of
Distributed Volcanism—Characteristics, Processes, and Hazards
Edited by Michael P. Poland, Michael H. Ort, Wendy K. Stovall, R. Greg Vaughan, Charles B. Connor, and M. Elise Rumpf

Professional Paper 1890

U.S. Department of the Interior
U.S. Geological Survey

U.S. Geological Survey, Reston, Virginia: 2024

For more information on the USGS—the Federal source for science about the Earth, its natural and living resources, natural hazards, and the environment—visit https://www.usgs.gov/ or call 1–888–ASK–USGS (1–888–275–8747).

For an overview of USGS information products, including maps, imagery, and publications, visit https://store.usgs.gov/.

Any use of trade, firm, or product names is for descriptive purposes only and does not imply endorsement by the U.S. Government.

Although this information product, for the most part, is in the public domain, it also may contain copyrighted materials as noted in the text. Permission to reproduce copyrighted items must be secured from the copyright owner.

Suggested citation:
Rivera, T.A., Jicha, B.R., Kirby, S., and Peacock, H.B., 2024, Temporal, spatial, and chemical evolution of Quaternary high-silica rhyolites in the Mineral Mountains, Utah, chap. K *of* Poland, M.P., Ort, M.H., Stovall, W.K., Vaughan, G.R., Connor, C.B., and Rumpf, M.E., eds., Distributed volcanism—Characteristics, processes, and hazards: U.S. Geological Survey Professional Paper 1890, 19 p., https://doi.org/10.3133/pp1890K.

ISSN 2330-7102 (online)

Acknowledgments

Wes Hildreth, Michael McCurry, Michael Ort, and Michael Poland contributed to the improvement of the manuscript. Barbara Nash is thanked for numerous discussions about Utah volcanism. Additional field and laboratory support was provided by Stacy Henderson, McKenna Holliday, Emily Kleber, Robert Biek, Peter Lippert, Sarah Lambart, and Christophe Brosson. This work was supported by the National Science Foundation Earth Sciences Division (EAR) Petrology and Geochemistry Program (grants EAR-1940305 and EAR-1940266), Association for Women Geoscientists, Geological Society of America, and Myriad Genetics.

Contents

Figures

Tables

Conversion Factors

International System of Units to U.S. customary units

Multiply	By	To obtain
	Length	
kilometer (km)	0.6214	mile (mi)
	Volume	
cubic kilometer (km^3)	0.2399	cubic mile (mi^3)

Datum

Vertical coordinate information is referenced to the North American Vertical Datum of 1988 (NAVD 88).

Horizontal coordinate information is referenced to World Geodetic System of 1984 (WGS 84).

Abbreviations

FeO^T	total iron as FeO
Ga	giga-annum
ka	kilo-annum
k.y.	thousand years (duration)
Ma	mega-annum
MSWD	mean square of weighted deviates
m.y.	million years (duration)
ppm	part per million
REE	rare earth element
σ	standard deviation

Distributed Volcanism—Characteristics, Processes, and Hazards
Edited by Poland, Ort, Stovall, Vaughan, Connor, and Rumpf
Professional Paper 1890

Chapter K

Temporal, Spatial, and Chemical Evolution of Quaternary High-Silica Rhyolites in the Mineral Mountains, Utah

By Tiffany A. Rivera,[1] Brian R. Jicha,[2] Stefan Kirby,[3] and Hannah B. Peacock[4]

Abstract

The Mineral Mountains in southwestern Utah are a structurally controlled core complex at the confluence of the Colorado Plateau and the Basin and Range physiographic provinces. Aside from hosting Utah's largest batholith, the Mineral Mountains host some of the State's youngest high-silica rhyolites, which have been linked to a magma source that is presently being utilized as an enhanced geothermal system. The high-silica rhyolites take the form of effusive lavas and domes, and explosive products are rare. Previous K-Ar dating of these Pleistocene rhyolites placed eruptions between about 790 and 500 kilo-annum (ka) with contemporaneous basalts erupting in the valley to the east of the Mineral Mountains. Large uncertainties on these ages obscured the tempo of eruptions and thus hindered attempts to constrain the timescales of the petrogenetic processes that produced the rhyolites. In this study, we build on previous studies conducted in the 1970s and 1980s by using new geochronologic and geochemical data to investigate the temporal and spatial evolution of the youngest phase of volcanism in the Mineral Mountains. We identify two major eruptive periods, from approximately 850 to 750 ka and from approximately 590 to 480 ka. The older phase is characterized by the eruption of several basaltic lavas, two obsidian flows, and a series of coalescing porphyritic rhyolite domes. The younger phase included the eruption of six evolved high-silica rhyolite domes and one pyroclastic deposit, followed by the eruption of trachyandesite in the adjacent valley to the east. Whole-rock geochemical data indicate that the rhyolites can be divided into three chemical groups, with more evolved compositions erupting through time. The youngest rhyolites along the range crest have the lowest total iron and TiO_2 concentrations and the highest incompatible element concentrations, indicative of increasing differentiation with time and elevation. Improved precision on the eruption ages indicates a recurrence interval of approximately 20 thousand years. The eruptive flux for both periods of rhyolitic volcanism is about 0.01 cubic kilometers per thousand years, which is less than the magma resurgence flux rates for syn-caldera and post-caldera eruptions of the Valles Caldera and Yellowstone Caldera volcanic systems. Collectively, these geochemical, geochronological, and volumetric data may facilitate a better understanding of heat flux and the longevity of magmatic sources related to geothermal resources in similar small-volume, silicic systems.

Introduction

Quaternary monogenetic basaltic volcanism is widespread in the southwestern United States, consisting of more than 2,200 volcanoes within 37 volcanic fields (Valentine and others, 2021). However, Quaternary rhyolitic volcanism across this region is even sparser, with the largest and possibly most studied being the Valles Caldera complex in New Mexico (Smith and others, 1970; Spell and Harrison, 1993; Nasholds and Zimmerer, 2022). To date, there are few studies that have focused on the petrogenetic relations of bimodal volcanism within an anorogenic setting, largely owing to the paucity of small-volume rhyolites within monogenetic volcanic fields (Smith and Nemeth, 2017). In predominantly basaltic settings, monogenetic volcanism refers to batches of magmas that rise quickly from the mantle to the surface, with minimal crustal interaction during ascent, resulting in a simple subsurface plumbing system (Smith and Nemeth, 2017). In non-basaltic settings, the plumbing systems of silicic magmas may be more intricate, extensive, and chemically variable and are often related to caldera-forming eruptions. In these systems, monogenetic volcanism consists of lavas fed by small-volume batches of melt derived from a common upper crustal reservoir (Smith and Nemeth, 2017). The Mineral Mountains are an example of distributed volcanism, which refers to eruptions from scattered vents rather than a central vent.

Within the Mineral Mountains of southwestern Utah, numerous small-volume Quaternary rhyolitic volcanic rocks offer an opportunity to examine the timing and chemical evolution of such volcanism. The Mineral Mountains are unique among Quaternary volcanic fields in Utah because they (1) host an active geothermal system (Nielson and others, 1978, 1986), (2) have the upper to middle crustal basement exposed beneath the volcanic field (Coleman and Walker, 1992), (3) contain a substantial number of high-silica rhyolites that are

[1]University of Missouri-Columbia.

[2]University of Wisconsin-Madison.

[3]Utah Geological Survey.

[4]Westminster University; now at Idaho National Laboratory.

some of the youngest in Utah, and (4) erupted contemporaneous basalts to andesites in the neighboring valley. Furthermore, the dominantly basaltic Black Rock Desert volcanic field (Condie and Barsky, 1972; Johnsen and others, 2010), located in the Sevier Desert to the north and east of the Mineral Mountains, is classified as having a moderate threat level by a U.S. Geological Survey analysis (Ewert and others, 2018).

Whereas many studies of Utah's Quaternary volcanism have focused on the geographic distribution of erupted units and the overall geochemical evolution of volcanism through time (for example, Best and others, 1980; Biek and others, 2010; Johnsen and others, 2010), this study presents new $^{40}Ar/^{39}Ar$ ages for nine <1 mega-annum (Ma) rhyolites of the Mineral Mountains and four mafic lavas that erupted in the valley to the east to establish an eruptive chronology. The new eruption ages allow us to examine the chemical and spatial migration of rhyolitic volcanism in the mountain range, establish a recurrence interval, and calculate magmatic flux rates. This information can assist in future assessments of eruption risk within Utah's Basin and Range Province.

Geologic Setting

The Black Rock Desert volcanic field is situated near the boundary between the Colorado Plateau and the Basin and Range physiographic provinces. The predominant volcanic products of the past 2.5 million years include high-silica rhyolites and subalkaline basalts, with minor intermediate rocks. Five subfields have been defined; from north to south, they are (1) Fumarole Butte, (2) Ice Springs, (3) Beaver Ridge, (4) Twin Peaks, and (5) Cove Fort (Nash, 1986). The Cove Fort subfield includes the high-silica rhyolites of the Mineral Mountains and the 1.3 to 0.3 Ma basalt to andesite flows in the valley east of the Mineral Mountains (fig. 1). This valley is informally known as the Cove Fort valley.

The predominant rock types of the Mineral Mountains are Oligocene to Miocene granitoids composing the Mineral Mountains batholith, with an exposed area of about 250 square kilometers. The batholith intruded into 1.725 giga-annum (Ga) banded gneiss, quartzite, and sillimanite schist (in the west and north) and Paleozoic and Mesozoic carbonates, quartzites, and other sedimentary rocks (south, north, and east sides of the range; Sibbett and Nielson, 1980; Coleman and Walker, 1992). Zircon U-Pb dates indicate much of the batholith was emplaced between 18 and 16 Ma with subsequent dike emplacement at approximately 9 Ma (Coleman and Walker, 1992; Coleman and others, 2001). Intrusions became more silicic with time and contain hornblende and biotite along with accessory titanite, apatite, allanite, and zircon (Coleman and Walker, 1992). Exhumation of the batholith has been estimated to have occurred between 10 and 8 Ma (Nielson and others, 1986; Coleman and others, 2001).

Pleistocene volcanism above the batholith produced two obsidian flows, a pyroclastic deposit consisting of ash-fall and ash-flow tuffs, and numerous monogenetic porphyritic rhyolite domes that vented mostly along the ridge crest (fig. 1), totaling approximately 15 cubic kilometers (km^3) (Nash, 1986). Previous K-Ar dating constrained eruptions between 860 and 540 kilo-annum (ka) (Lipman and others, 1978; Nash, 1986), and to the east of the range, the mafic flows of the Cove Fort valley are inferred to have erupted contemporaneously (Condie and Barsky, 1972; Best and others, 1980; Nash, 1986). Mafic crustal injections associated with the basalts of Cove Fort valley may have provided the necessary heat for rhyolite production in the Mineral Mountains; quenched basalt xenoliths present within some of the rhyolites indicate direct injection of mafic material into the silicic magma bodies (Nash, 1986). However, the large uncertainties of the K-Ar ages do not allow for temporal relations to be established among the rhyolites or between the rhyolites and adjacent mafic lavas.

Structural control may be responsible for the distribution of the pluton, rhyolite domes, and geothermal activity (Sibbett and Nielson, 1980). Pluton emplacement was oriented in a north-south direction, likely a result of east-west Basin and Range Province extension (Sibbett and Nielson, 1980). Structural control of the rhyolites is less defined, but the vents are distributed north-south along the ridge crest and are located at or near the contact between two types of granitoids within the batholith (Sibbett and Nielson, 1980). In the central Mineral Mountains, the Roosevelt Hot Springs Known Geothermal Resource Area hosts a 28-megawatt geothermal power plant that utilizes high conductive heat at relatively shallow depth (Nielson and others, 1978, 1986). Geothermal activity at Roosevelt Hot Springs is structurally controlled in that the west side of the range is bounded by the Opal Mound north-striking normal fault. High heat flow is well known in the region, with an average of 90 milliwatts per square meter (Chapman and others, 1978). It is likely that the heat at Roosevelt Hot Springs is derived from the igneous material that fed the Pleistocene rhyolite eruptions, which may also be linked to the mafic activity in the Cove Fort valley (Lipman and others, 1978). Two low-velocity zones, one as shallow as 5 kilometers (km), have been recognized and interpreted to be magma bodies (Ward and others, 1978; Robinson and Iyer, 1979); however, gravity and magnetic surveys do not indicate a low-density partial melt as the source of heat for the geothermal system (Ward and others, 1978).

Description of Units and Previous Geochronology

Nine Pleistocene lava domes have been identified across the Mineral Mountains, most of them at the highest elevations along the ridge crest. Physical characteristics and outcrop patterns are detailed by Lipman and others (1978) and Nash (1976, 1986) and are briefly summarized here. Mineral assemblages across all domes are similar, consisting of phenocrysts of quartz, plagioclase, and sanidine. In general, the domes at the highest elevations have 1–2 percent phenocrysts, whereas domes in the middle of the mountain range have 10–12 percent crystals, contain minor amounts of biotite (<1 percent), and trace amounts of titanite and zircon. Compositional zoning is common in feldspars and quartz and all domes contain two feldspars, with approximate compositions of 65 percent orthoclase (Or_{65}) and 80 percent albite (Ab_{80}) (Evans and Nash, 1978; Nash, 1986).

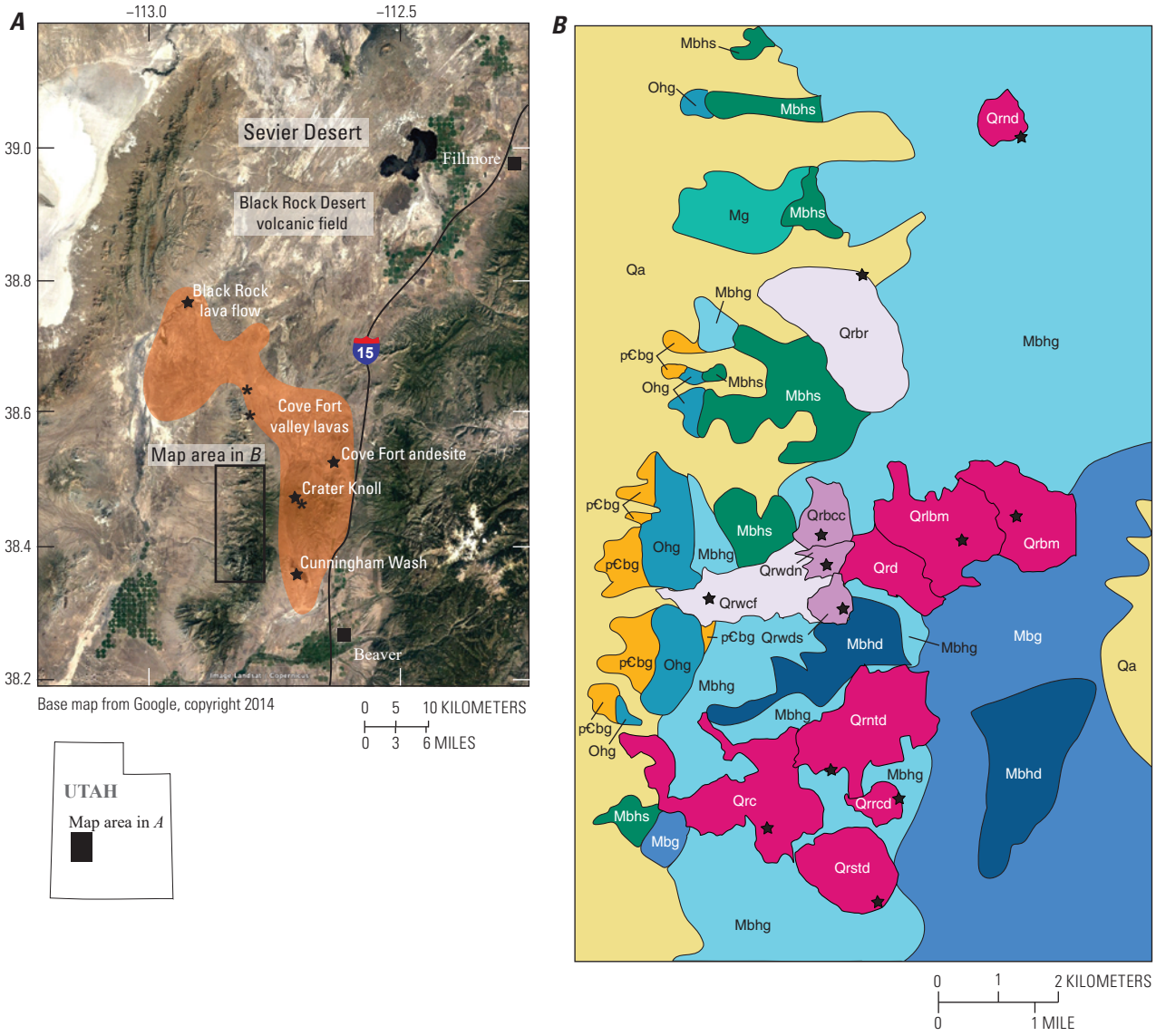

EXPLANATION

Quaternary surficial deposit
- Qa — Alluvium

Quaternary rhyolite—High domes
- Qrstd — Rhyolite of South Twin dome
- Qrntd — Rhyolite of North Twin dome
- Qrrcd — Rhyolite of Ranch Canyon dome
- Qrc — Tuff and rhyolite of Ranch Canyon
- Qrnd — Rhyolite of North dome
- Qrbm — Rhyolite of Bearskin Mountain
- Qrlbm — Rhyolite of Little Bearskin Mountain
- Qrd — Rhyolite, undifferentiated

Quaternary rhyolite—Middle domes
- Qrwdn — Rhyolite of north Wildhorse Canyon dome
- Qrwds — Rhyolite of south Wildhorse Canyon dome
- Qrbcc — Rhyolite of Big Cedar Cove

Quaternary rhyolite—Obsidian flows
- Qrwcf — Rhyolite and tuff of Wildhorse Canyon
- Qrbr — Rhyolite of Bailey Ridge

Miocene and Oligocene intrusive rock
- Mg — Granite dike
- Mbg — Biotite granite
- Mbhs — Biotite-hornblende syenite
- Mbhd — Biotite-hornblende diorite
- Mbhg — Biotite-hornblende granite
- Ohg — Hornblende granodiorite

Precambrian metamorphic rock
- pЄbg — Biotite gneiss

Contact

Mafic vent

Sample site

Figure 1. Map of the study area in southwestern Utah. *A*, Regional map showing the study area. *B*, Simplified geologic map of the Mineral Mountains (modified from Kirby, 2019).

Six of the youngest domes, herein referred to as the high domes, span more than 10 km along the Mineral Mountains range crest. Three domes are identified in Ranch Canyon: North Twin Flat Mountain, South Twin Flat Mountain, and Ranch Canyon dome. Based on the degree of dissection, North and South Twin Flat Mountain domes were assumed to be among the oldest erupted in this canyon, with a K-Ar age of 500±70 ka (all uncertainties are reported at 2 standard deviations [2σ]) for South Twin Flat Mountain (Lipman and others, 1978). Nash (1986) reported ages of 690±80, 630±60, and 620±80 ka for pumice from South Twin Flat Mountain and ages of 730±120 and 680±60 ka for North Twin Flat Mountain. Ranch Canyon dome produced anomalously old ages of 7.39±0.78 and 6.55±0.46 Ma (Nash, 1986).

In Wildhorse Canyon, Bearskin Mountain (750±100 and 600±120 ka) and Little Bearskin Mountain (610±50 ka) domes were thought to be the youngest lavas based on degree of dissection. Nash (1986) reported ages of 620±220 ka for Bearskin Mountain and 740±940 ka for Little Bearskin Mountain, which are similar to those of Lipman and others (1978). The 800±80 ka (Nash, 1986) Big Cedar Cove dome is located down-canyon (west) from Bearskin and Little Bearskin Mountains. North Wildhorse Canyon dome and south Wildhorse Canyon dome are two smaller domes located south of Big Cedar Cove dome (fig. 1). We designate these central domes (Big Cedar Cove dome, north Wildhorse Canyon dome, and south Wildhorse Canyon dome) into a group called the "middle domes." Prior to this study, no isotopic ages had been determined for either Wildhorse Canyon domes.

The obsidian flows of Bailey Ridge and Wildhorse Canyon are high-silica rhyolite flows located along the western front of the Mineral Mountains (Lipman and others, 1978; Nash, 1986). Vents for these two flows have not been identified, but the extension of the Wildhorse Canyon flow up-canyon toward the middle domes indicates either the vent is buried by a younger flow or that the source of one of those domes also produced the flow (Nash, 1976). The Bailey Ridge obsidian flow is considered to be the oldest of the Pleistocene lavas, with a reversed magnetic polarity and K-Ar age of 860±140 ka (weighted mean of two analyses by Lipman and others, 1978, and Nash, 1986). No previous geochronology exists for the Wildhorse Canyon obsidian flow, but the reversed polarity and chemical similarity to the Bailey Ridge obsidian flow led Lipman and others (1978) to assume a similar age.

One pyroclastic deposit (0.4 km^3; Nash, 1976, 1986) is exposed within Ranch Canyon (fig. 1). The tuff of Ranch Canyon is characterized by a basal proximal fallout deposit with large (>10 centimeter) pumice blocks and a variety of lithic clasts, including glassy and snowflake obsidian, rhyolite, and granite. Above the fallout deposit is a sequence of normally graded pumice lapilli, capped by a series of cross-bedded surge deposits. Lipman and others (1978) obtained a K-Ar age of 700±40 ka from an obsidian block hosted within the basal tuff, placing a maximum age on the deposit.

Whereas the majority of the Mineral Mountains is of felsic composition, the Cove Fort subfield of the Black Rock Desert volcanic field produced several mafic cinder cones and lava flows at the north end of the range (fig. 1). A tholeiitic basaltic lava flow in the western part of the Cove Fort subfield, referred to informally as the Black Rock flow by Crecraft and others (1981), has dominant olivine and plagioclase and intergranular clinopyroxene. Referred to herein as the Black Rock lava flow, this lava flowed northwest about 25 km along the ancestral Cove Creek (Nash, 1986). Two K-Ar ages of 1.32±0.18 Ma and 920±520 ka were obtained from two different samples of this lava (Nash, 1986). To the east of the Mineral Mountains, the Cove Fort subfield is characterized by basaltic andesites and trachyandesites (55 to 62 weight percent SiO_2; Nash, 1986). The oldest of these erupted around 1.1 Ma, with additional eruptions at 500 and 300 ka (Best and others, 1980; Nash, 1986).

Materials and Methods

Hand samples for geochemical and $^{40}Ar/^{39}Ar$ analyses were collected from nine rhyolite domes, two obsidian flows, and one pyroclastic fallout deposit from the Mineral Mountains. Mafic to intermediate lava samples from Cove Fort valley include the Black Rock lava flow, a trachyandesite flow in the eastern part of the Cove Fort subfield (herein referred to as the Cove Fort andesite), a basaltic andesite flow at Crater Knoll, and a basaltic andesite at Cunningham Wash (fig. 1, table 1). Glass was separated from the obsidian flows. Plagioclase was isolated from the Black Rock lava flow, and inclusion-free groundmass was separated from the Cove Fort andesite. Feldspar crystals were extracted from the dome lavas. These separates were irradiated along with sanidine from the rhyolite of Alder Creek as the neutron fluence monitor (1.1864 Ma; Rivera and others, 2013; Jicha and others, 2016) in the cadmium-lined in-core irradiation tube at the Oregon State University TRIGA reactor. Dating by $^{40}Ar/^{39}Ar$ was performed at the University of Wisconsin-Madison using a 55-watt CO_2 laser coupled to a Nu Instruments Noblesse multi-collector mass spectrometer following methods of Jicha and others (2016). Purified glass, groundmass, and plagioclase separates were incrementally heated, whereas single feldspar crystals were analyzed by either total fusion or incremental heating (table 1). All Alder Creek sanidine monitors were analyzed via total fusion. Ages were calculated using the decay constants of Min and others (2000), and uncertainties are reported at the 2σ level and include error contributions from the irradiation parameter *J*.

Whole-rock major, trace, and rare earth element chemical analyses were obtained via X-ray fluorescence and inductively coupled plasma mass spectrometry at either the Peter Hooper GeoAnalytical Laboratory at Washington State University or the Hamilton Analytical Laboratory at Hamilton College. Analytical procedures follow those of Knaack and others (1994). Volumes for the obsidian flows and domes were estimated using a 1-meter digital elevation model (U.S. Geological Survey, 2021) and QGIS analytical tools (http://www.qgis.org). The volumes

Table 1. Summary of $^{40}Ar/^{39}Ar$ data for samples analyzed in this study.

[Ages calculated relative to 1.1864 mega-annum (Ma) sanidine of the rhyolite of Alder Creek using decay constants of Min and others (2000). Atmospheric $^{40}Ar/^{36}Ar$ = 298.56±0.62 (Lee and others, 2006). # is number of incremental heating experiments conducted per sample used to calculate the weighted mean plateau age. *n*/*N* is number of plateau steps per number of total incremental heating steps, or number of dates used in the calculation of the weighted mean per total number of single crystal fusion dates. Interfering isotope production ratios are $(^{40}Ar/^{39}Ar)_K$ = 0.00073±0.00009, $(^{38}Ar/^{39}Ar)_K$ = 0.01215±0.00003, $(^{37}Ar/^{39}Ar)_K$ = 0.000224±0.000016, $(^{39}Ar/^{37}Ar)_{Ca}$ = 0.000702±0.000012, $(^{38}Ar/^{37}Ar)_{Ca}$ = 0.000020±0.000001, and $(^{37}Ar/^{39}Ar)_{Ca}$ = 0.0002702±0.0000004. $^{40}Ar/^{36}Ar_i$, $^{40}Ar/^{36}Ar$ isochron intercept; ka, kilo-annum; MSWD, mean square of weighted deviates; %, percent; 2σ, two standard deviations; —, not applicable]

Group	Sample	Location	Material	#	$^{40}Ar/^{36}Ar_i$ ±2σ (ka)	Isochron age ±2σ (ka)	*n*/*N*	^{39}Ar %	MSWD	Plateau age ±2σ (ka)
Mafic lava	21BRD-25	Cove Fort andesite	Groundmass	1	299±4	409±99	29/48	60	0.26	417±23
High dome	17MMST-1	South Twin Flat Mountain	Sanidine	7	297±3	479±9	36/49	87	0.58	483±4
High dome	17MMRCD-1[a]	Ranch Canyon dome	Sanidine		—	—	14/20	—	1.53	501±4
High dome	17MMND-1	North dome	Sanidine	8	298±2	514±7	50/57	97	0.18	520±4
High dome	17MMBM-2	Bearskin Mountain	Sanidine	5	294±10	537±9	13/26	87	0.48	539±4
High dome	17MMLBM-1	Little Bearskin Mountain	Sanidine	3	303±24	578±17	16/17	96	0.88	588±7
Mafic lava	22BRD-53	Cunningham Wash	Groundmass	1	300±3	724±52	29/42	84	0.71	748±14
Mafic lava	22BRD-54	Crater Knoll	Groundmass	1	300±4	736±53	21/36	71	0.63	754±14
Middle dome	17MMWDS-1[b]	South Wildhorse Canyon dome	Sanidine		—	—	8/11	—	0.86	758±6
Middle dome	17MMWDN-1	North Wildhorse Canyon dome	Sanidine	3	298±4	767±6	18/19	95	0.33	766±3
Obsidian flow	17MMWCF-1	Wildhorse Canyon	Glass	1	301±8	772±55	33/34	98	1.07	786±5
Obsidian flow	17MMBR-1	Bailey Ridge	Glass	1	307±11	848±5	12/17	77	1.20	851±3
Mafic lava	18BRDBR-1	Black Rock lava flow	Plagioclase	2	299±1	856±39	61/65	92	0.91	865±30

[a]Data for rhyolite of Ranch Canyon dome were obtained via single crystal fusions. Age is a weighted mean of the 14 youngest $^{40}Ar/^{39}Ar$ dates.

[b]Data for rhyolite of south Wildhorse Canyon dome were obtained via single crystal fusions. Age is a weighted mean of the 8 youngest $^{40}Ar/^{39}Ar$ dates.

were calculated using the area of a polygon and the difference in topographic elevation assuming a constant base plane of reference for each dome or flow. The base plane of reference elevation was determined as the lowest elevation of the lava flow and assumed to be a level surface (in other words, no accounting for unknown subflow or subdome paleotopography). This technique has been used to estimate the volumes of rhyolite domes for Valles Caldera in New Mexico (Nasholds and Zimmerer, 2022) and the Coso volcanic field in California (Burgess and others, 2021).

Results

Whole-Rock Major, Trace, and Rare Earth Element Geochemistry

All felsic samples analyzed in this study are high-silica rhyolites, with normalized volatile-free concentrations that are in a narrow range between 76.8 and 78.0 weight percent SiO_2, 0 and 0.2 weight percent MgO, and 8.2 and 9.2 weight percent total alkalis ($Na_2O + K_2O$) (fig. 2*A*, table 2). Despite the limited range in SiO_2 and MgO concentration, other major element oxides vary. The high domes have higher Al_2O_3 concentrations but lower TiO_2 and total iron as FeO (FeO^T) than the obsidian flows and middle domes. The obsidian flows have the highest TiO_2 concentrations. The distinction of the three groups of rhyolites is also apparent in trace and rare earth element concentrations. Incompatible elements, such as Rb and Nb, vary widely among the rhyolites, such that the obsidian flows have the lowest Nb concentrations (23–24 parts per million [ppm]) and the middle dome lavas (27–28 ppm) and high dome lavas (36–44 ppm) have higher concentrations. This pattern is also observed for Rb (fig. 2*C*), but Eu systematically decreases from obsidian to the middle dome lavas and finally to the high dome lavas (fig. 2*G*). Trace element ratios, such as Y/Yb and Ba/Sr, also demonstrate the chemical distinction between the three groups.

Chondrite-normalized rare earth element (REE) patterns additionally demonstrate the chemical distinction between the obsidian flows, middle domes, and high dome lavas and tuff (fig. 3; table 3). The obsidian flows are nearly indistinguishable from each other, are more enriched in light REE, and have a less negative Eu anomaly relative to lavas of the other groups. The high dome lavas have a strong negative Eu anomaly, and the middle REEs form a saddle where heavy REEs are more enriched than middle REEs. The REE patterns of the middle dome lavas are nearly identical, and the saddle shape is present but not as prominent.

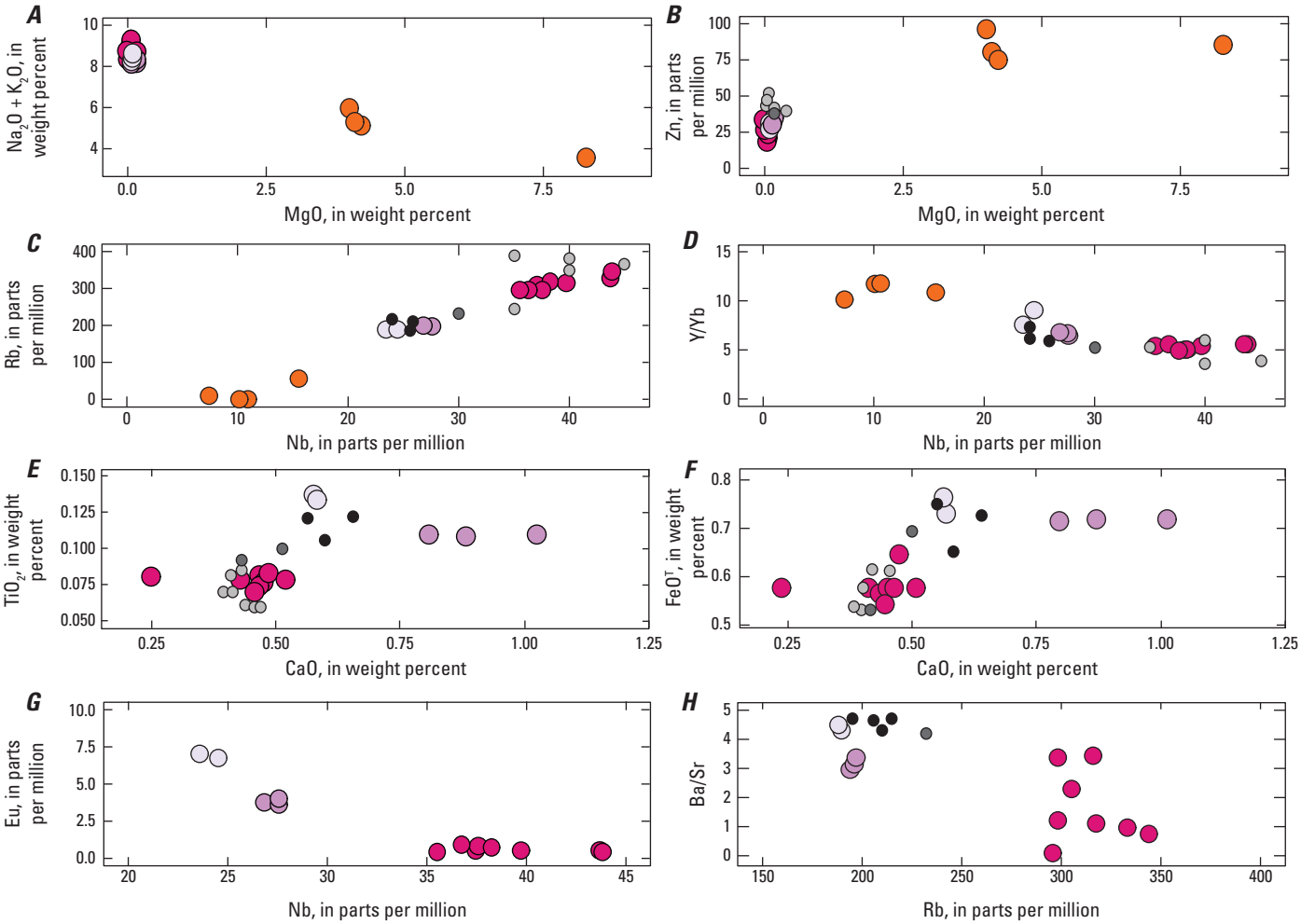

Figure 2. Select Harker and bivariate trace element plots for the high-silica rhyolites of the Mineral Mountains and neighboring basalts, southwestern Utah. All oxides are calculated to 100 weight percent on an anhydrous basis. Data from this study and Nash (1986).

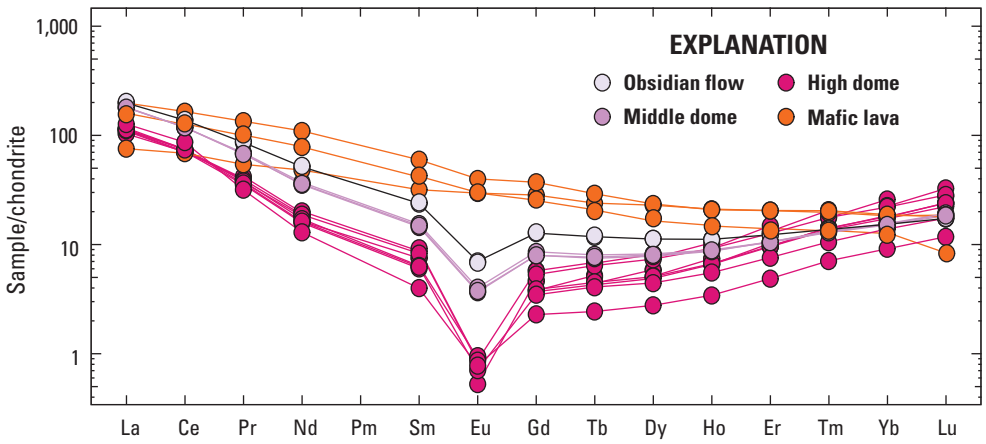

Figure 3. Chondrite-normalized rare earth element plot of Mineral Mountains rhyolites and neighboring mafic lavas in southwestern Utah. Chondrite values from Sun and McDonough (1989).

Table 2. Whole-rock major element data for rhyolites of the Mineral Mountains and neighboring mafic lavas, southwestern Utah.

[Concentrations determined via X-ray fluorescence. Concentrations are normalized to 100 percent; "original total" is the total before normalization. All iron is reported as FeO (FeO^T). LOI, loss on ignition; —, not determined]

Sample	Latitude (°N)	Longitude (°E)	Location	Concentration, in weight percent												
				SiO_2	TiO_2	Al_2O_3	FeO^T	MnO	MgO	CaO	Na_2O	K_2O	P_2O_5	Total	Original total	LOI
Obsidian flows																
17MMBR-1	38.488	−112.811	Bailey Ridge	77.46	0.13	12.56	0.73	0.05	0.06	0.57	3.42	5.02	0.01	100.00	98.94	0.29
17MMWCF-1	38.445	−112.849	Wildhorse Canyon	77.41	0.14	12.56	0.76	0.05	0.07	0.62	3.34	5.04	0.01	100.00	98.73	1.12
Middle domes																
17MMBCCD-1	38.456	−112.823	Big Cedar Cove dome	77.31	0.11	12.50	0.72	0.06	0.07	0.87	3.68	4.67	0.02	100.00	98.62	1.07
17MMWDN-1	38.449	−112.821	North Wildhorse Canyon dome	77.08	0.11	12.48	0.72	0.06	0.15	1.01	3.36	5.01	0.03	100.00	96.52	3.22
17MMWDS-1	38.440	−112.818	South Wildhorse Canyon dome	77.36	0.11	12.56	0.72	0.06	0.06	0.80	3.49	4.83	0.01	100.00	96.71	2.54
High domes																
17MMND-1	38.512	−112.790	North dome	76.87	0.08	12.74	0.58	0.06	0.05	0.51	4.41	4.70	0.01	100.00	90.40	8.89
17MMBM-2	38.457	−112.786	Bearskin Mountain	77.32	0.08	12.77	0.58	0.08	0.12	0.46	3.92	4.66	0.02	100.00	98.58	0.94
17MMLBM-1	38.454	−112.794	Little Bearskin Mountain	77.68	0.08	12.77	0.58	0.07	0.01	0.24	3.92	4.65	0.01	100.00	99.10	0.28
17MMNTD-1	38.424	−112.819	North Twin Flat Mountain	77.33	0.08	12.86	0.57	0.08	0.01	0.41	3.96	4.68	0.01	100.00	98.90	0.51
17MMRCD-1	38.416	−112.809	Ranch Canyon dome	77.47	0.08	12.78	0.57	0.08	0.02	0.45	4.02	4.51	0.02	100.00	99.23	0.36
17MMST-1	38.404	−112.813	South Twin Flat Mountain	77.17	0.07	12.87	0.55	0.07	0.06	0.45	4.22	4.52	0.02	100.00	98.68	0.75
Pyroclastic rocks																
17MMRC-1	38.411	−112.823	Tuff of Ranch Canyon (pumice)	77.51	0.08	12.76	0.58	0.08	0.01	0.45	3.86	4.66	0.01	100.00	95.32	4.30
17MMRC-2	38.143	−112.818	Tuff of Ranch Canyon (pumice)	77.22	0.08	12.94	0.65	0.08	0.04	0.48	3.73	4.79	0.01	100.00	92.54	6.98
Mafic-intermediate lava flows																
18BRDBR-1[a]	38.768	−112.908	Black Rock lava flow	49.42	1.31	17.04	9.79	0.17	8.27	10.05	3.03	0.63	0.30	100.00	99.43	—
21BRD-25[a]	38.529	−112.659	Cove Fort andesite	57.10	1.36	15.81	8.21	0.14	3.96	6.71	3.67	2.31	0.74	100.00	98.43	0.70
22BRD-53[a]	38.358	−112.700	Cunningham Wash	56.18	1.04	17.82	7.04	0.11	4.18	8.13	3.51	1.67	0.32	100.00	99.16	0.19
22BRD-54[a]	38.482	−112.736	Crater Knoll	55.94	1.06	17.94	7.26	0.11	4.20	8.01	3.43	1.72	0.33	100.00	99.06	0.20

[a]Analyzed at Hamilton Analytical Laboratory; all others analyzed at Washington State University.

Table 3. Whole-rock trace and rare earth element data for rhyolites of the Mineral Mountains and neighboring mafic lavas, southwestern Utah.

[Concentrations for Ni, Cr, Sc, V, Ba, Rb, Sr, Zr, Y, and Nb determined via X-ray fluorescence; the rest were determined via inductively coupled plasma mass spectrometry]

Sample	Concentration, in parts per million																												
	Ni	Cr	Sc	V	Ba	Rb	Sr	Zr	Y	Nb	La	Ce	Pr	Nd	Sm	Eu	Gd	Tb	Dy	Ho	Er	Tm	Yb	Lu	Th	Hf	Ta	U	Pb	Cs
Obsidian flows																														
17MMBR-1	9	4	0	17	162	186	38	108	20	24	46.90	84.28	8.18	24.09	3.65	0.41	2.62	0.44	2.85	0.63	2.03	0.35	2.60	0.44	22.69	4.38	1.82	5.63	32.68	3.35
17MMWCF-1	1	2	4	3	174	182	44	109	20	23	47.81	84.44	8.41	24.65	3.72	0.39	2.67	0.45	2.86	0.63	2.02	0.35	2.54	0.44	22.66	4.33	1.79	5.53	33.64	3.21
Middle domes																														
17MMBCCD-1	0	3	3	1	106	195	35	99	18	28	42.88	72.67	6.45	16.51	2.22	0.21	1.64	0.28	1.98	0.49	1.75	0.33	2.62	0.48	24.84	4.52	1.96	6.20	35.00	3.64
17MMWDN-1	0	2	2	4	121	195	40	96	18	27	42.58	72.49	6.40	16.74	2.28	0.22	1.64	0.29	2.04	0.50	1.74	0.33	2.57	0.47	24.00	4.38	1.91	5.92	33.64	3.59
17MMWDS-1	2	2	4	4	113	196	33	99	18	28	42.82	72.32	6.57	17.31	2.36	0.23	1.76	0.30	2.08	0.50	1.75	0.34	2.65	0.49	24.68	4.42	1.97	6.03	34.22	3.56
High domes																														
17MMND-1	7	3	0	0	3	293	6	85	16	36	26.40	43.40	3.37	7.39	0.92	0.02	0.76	0.16	1.24	0.37	1.58	0.35	2.94	0.57	35.55	4.32	2.44	8.05	36.63	4.13
17MMBM-2	1	3	3	2	17	318	10	92	12	38	26.90	45.74	3.44	7.59	0.96	0.04	0.71	0.15	1.13	0.31	1.26	0.27	2.36	0.44	38.26	5.09	2.62	8.99	38.71	5.59
17MMLBM-1	1	3	3	1	8	300	2	96	8	38	30.10	52.90	3.01	6.06	0.61	0.05	0.47	0.09	0.70	0.19	0.81	0.18	1.55	0.30	33.94	5.12	2.46	8.72	36.39	4.38
17MMNTD-1	0	2	3	3	5	316	1	96	16	40	27.70	45.69	3.61	8.00	0.98	0.03	0.80	0.17	1.29	0.38	1.60	0.36	3.06	0.61	39.67	5.23	2.74	9.67	40.18	6.05
17MMRCD-1	0	2	4	1	7	345	6	101	22	44	24.46	43.30	3.74	8.77	1.27	0.02	1.09	0.24	1.87	0.52	2.09	0.45	3.74	0.72	41.90	5.55	3.15	10.22	39.37	6.65
17MMST-1	4	3	3	3	5	329	3	100	24	44	24.62	42.75	3.83	9.16	1.33	0.03	1.19	0.26	2.06	0.59	2.46	0.53	4.39	0.83	42.43	5.64	3.20	10.20	39.05	4.44
Pyroclastic rocks																														
17MMRC-1	10	4	2	2	9	302	2	92	17	38	26.58	44.17	3.52	7.64	0.98	0.03	0.78	0.16	1.30	0.37	1.58	0.36	3.02	0.59	38.15	5.00	2.63	9.31	37.55	5.89
17MMRC-2	13	4	3	3	9	298	4	92	17	38	27.40	45.21	3.74	8.51	1.15	0.05	0.97	0.20	1.50	0.42	1.70	0.37	3.12	0.61	38.32	4.99	2.57	9.13	36.87	5.98
Mafic-intermediate lava flows																														
18BRDBR-1[a]	142	162	30	204	307	10	452	121	32	7	17.90	41.97	5.16	22.48	4.86	1.72	5.84	0.90	5.83	1.20	3.39	0.52	3.20	0.45	1.05	3.07	0.38	0.25	3.00	0.09
21BRD-25[a]	38	26	19	168	909	56	564	200	34	16	46.87	101.11	12.80	51.33	9.14	2.32	7.64	1.09	5.98	1.18	3.38	0.50	3.12	0.47	5.94	4.80	0.93	1.36	13.18	0.99
22BRD-53[a]	68	105	18	159	814	30	865	77	25	10	34.85	72.24	8.83	33.97	5.96	1.62	4.87	0.69	4.02	0.80	2.20	0.33	2.08	0.22	3.79	3.69	0.49	0.59	8.75	0.28
22BRD-54[a]	68	101	18	160	840	29	864	77	24	11	35.73	74.94	9.03	34.89	6.15	1.66	4.98	0.74	4.01	0.81	2.28	0.33	2.04	0.20	3.89	3.79	0.51	0.55	8.95	0.26

[a]Analyzed at Hamilton Analytical Laboratory; all others analyzed at Washington State University.

$^{40}Ar/^{39}Ar$ Geochronology

We obtained new $^{40}Ar/^{39}Ar$ ages for thirteen samples from rhyolites of the Mineral Mountains and mafic lavas from the adjacent Cove Fort valley. None of the samples show evidence of trapped excess argon and thus the plateau and weighted mean ages are used hereafter. Two incremental heating experiments of plagioclase from the Black Rock lava flow resulted in a weighted mean age of 865±30 ka. Groundmass analyses of two intermediate lavas, Crater Knoll and Cunningham Wash from the Cove Fort valley, produced plateau ages of 754±14 and 748±14 ka, respectively. Two incremental heating of trachyandesite groundmass from the Cove Fort andesite resulted in an age of 417±23 ka (fig. 4).

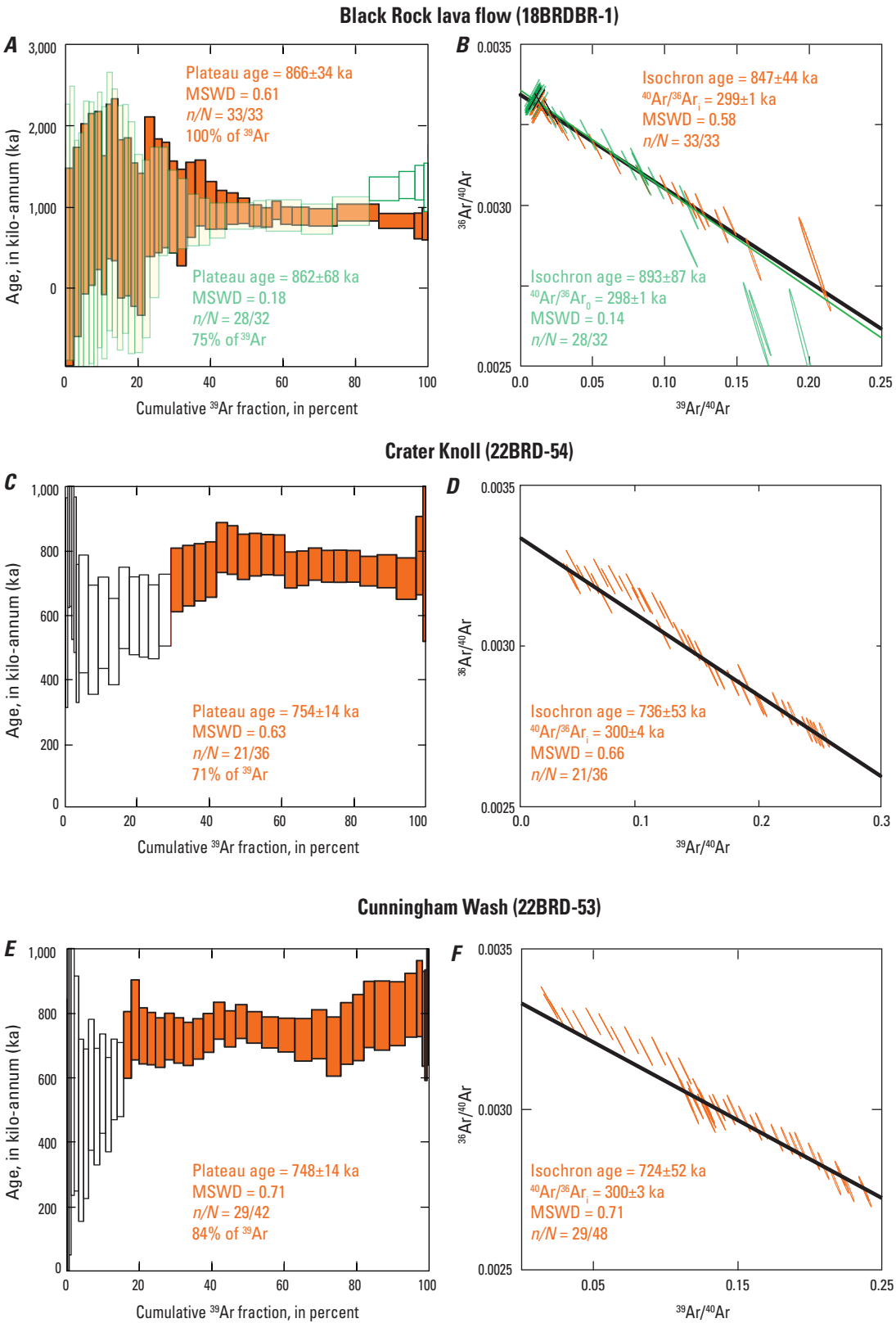

Figure 4 (pages 9 and 10). Age spectrum and inverse isochron plots for mafic to intermediate lavas from near the Mineral Mountains, southwestern Utah. Two analyses were made for sample 18BRDBR-1; the weighted mean of the two is given in table 1. Filled boxes on age spectrum plots represent steps included in the age calculation; open ones were excluded. Transparent colors allow overlap to be visible. $^{40}Ar/^{36}Ar_i$, isochron intercept; MSWD, mean square of weighted deviates; *n*/*N*, number of included analyses out of total analyses; %, percent.

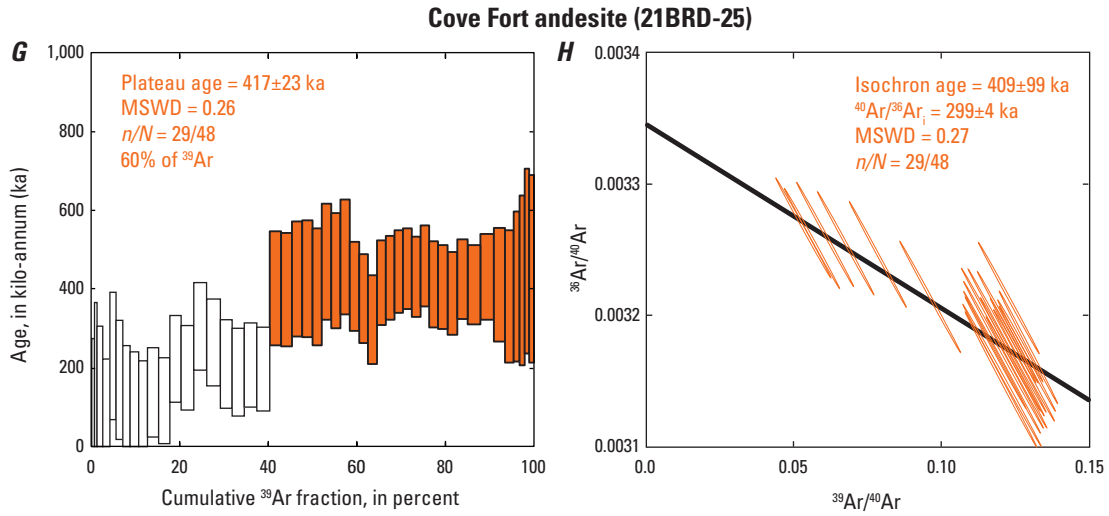

Figure 4 (pages 9 and 10).—Continued

Incremental heating of purified obsidian glass resulted in ages of 851±3 and 786±5 ka for the Bailey Ridge and Wildhorse Canyon obsidian flows, respectively (fig. 5). Plateaus include >75 percent of the $^{39}Ar_K$ released and isochron intercepts are within uncertainty of the atmospheric value. Three single feldspar grains from north Wildhorse Canyon dome produced a plateau that included >85 percent of the $^{39}Ar_K$ with ages between 768±5 and 765±7 ka (fig. 6). A weighted mean of these grains yields an age of 766±3 ka (mean square of weighted deviates [MSWD] = 0.33). Eight single-crystal fusion experiments

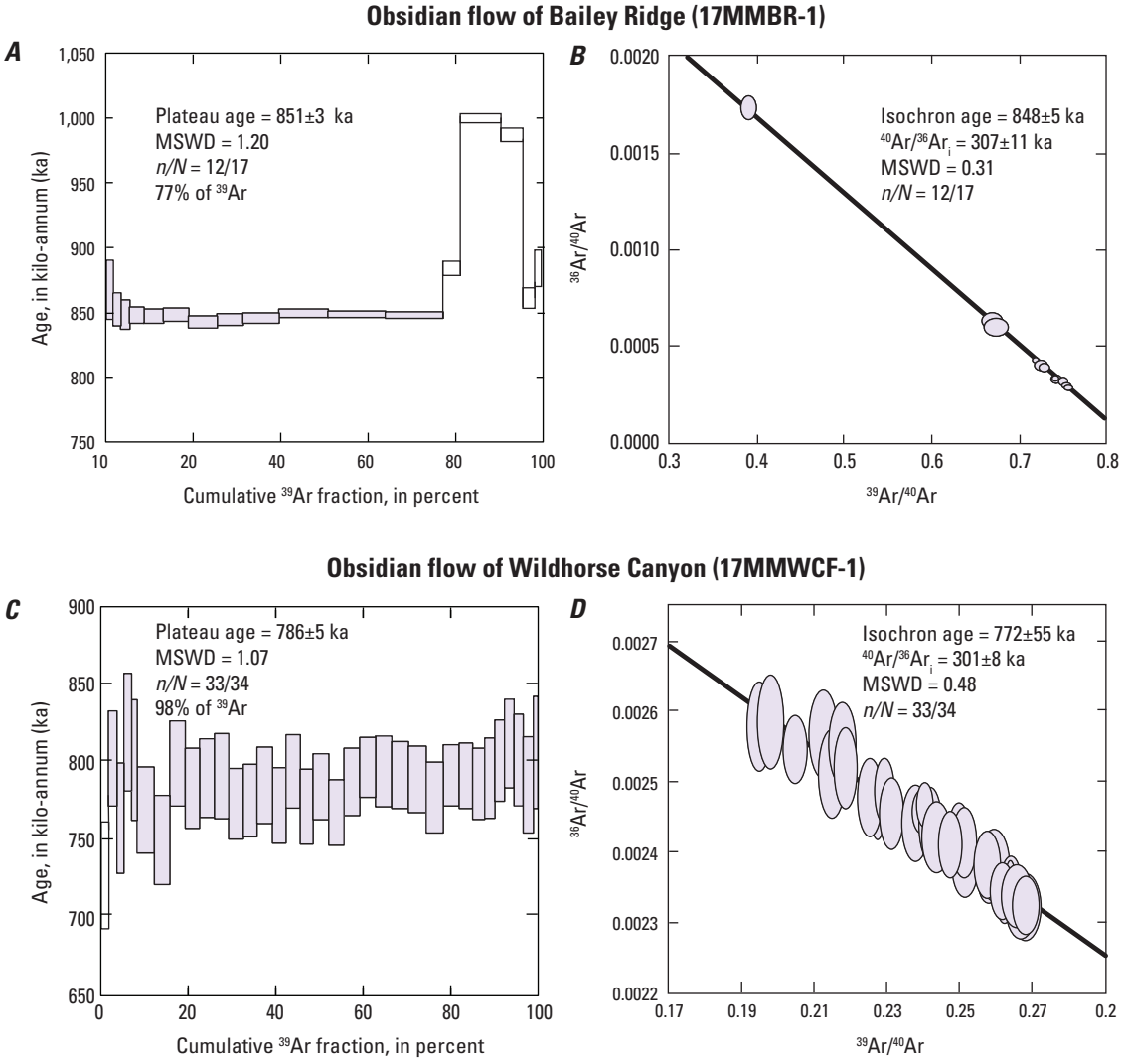

Figure 5. Age spectrum and inverse isochron plots for obsidian flows of Bailey Ridge and Wildhorse Canyon in the Mineral Mountains, southwestern Utah. Filled boxes on age spectrum plots represent steps included in the age calculation; open ones were excluded. $^{40}Ar/^{36}Ar_i$, isochron intercept; MSWD, mean square of weighted deviates; *n*/*N* = number of included analyses out of total analyses; %, percent.

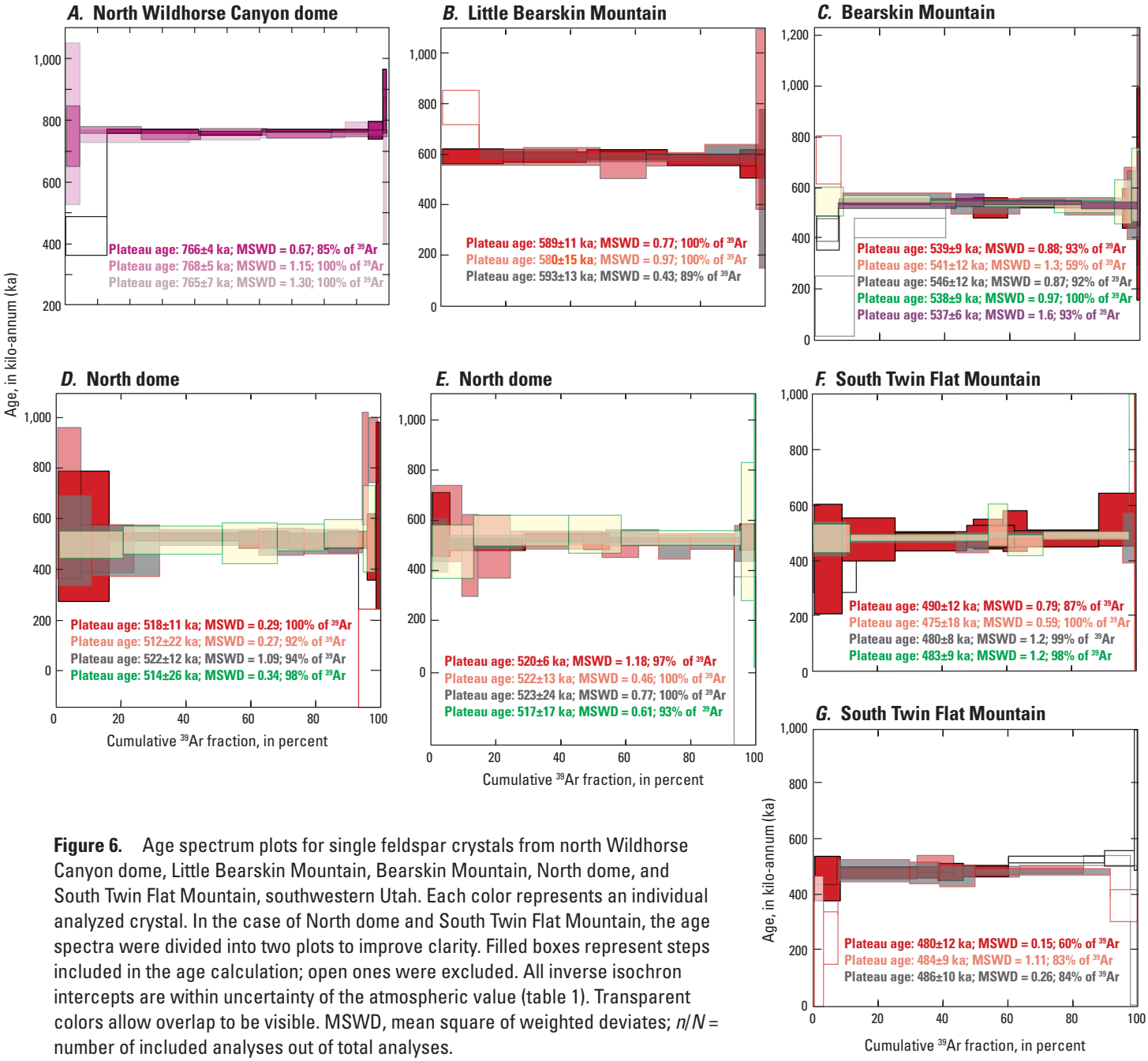

Figure 6. Age spectrum plots for single feldspar crystals from north Wildhorse Canyon dome, Little Bearskin Mountain, Bearskin Mountain, North dome, and South Twin Flat Mountain, southwestern Utah. Each color represents an individual analyzed crystal. In the case of North dome and South Twin Flat Mountain, the age spectra were divided into two plots to improve clarity. Filled boxes represent steps included in the age calculation; open ones were excluded. All inverse isochron intercepts are within uncertainty of the atmospheric value (table 1). Transparent colors allow overlap to be visible. MSWD, mean square of weighted deviates; *n*/*N* = number of included analyses out of total analyses.

from south Wildhorse Canyon dome yield a weighted mean age of 758±6 ka (MSWD = 0.86). Five of the high domes were dated for this study (fig. 6). Three grains from Little Bearskin Mountain produced plateau ages ranging from 593±13 to 580±15 ka. These result in a weighted mean age of 588±7 ka (MSWD = 0.88). Five grains from Bearskin Mountain produced plateau ages ranging from 546±12 to 537±6 ka, resulting in a weighted mean age of 539±4 ka (MSWD = 0.48). Eight feldspar crystals from North dome were individually step heated. Each grain produced a plateau with >90 percent of the $^{39}Ar_K$. Plateau ages range from 523±24 to 512±22 ka. A weighted mean of all grains results in an age of 520±4 ka (MSWD = 0.18). Single feldspar crystals from Ranch Canyon dome were analyzed via total fusion. The distribution of ages ranges from 548±8 to 489±26 ka. A weighted mean age for grains defining the youngest, dominant mode is 501±4 ka (MSWD = 1.53; number of dates in weighted mean calculation per total number of single crystal fusion dates [*n*/*N*] = 14/20; table 1). Seven grains from South Twin Flat Mountain produced plateau ages ranging from 490±12 to 480±12 ka, yielding a weighted mean age of 483±4 ka (MSWD = 0.58). Three additional units were analyzed (Big Cedar Cove dome, North Twin Flat Mountain, and pumice from the tuff of Ranch Canyon), but all produced inconclusive results. Ages are summarized in table 1.

Estimated Eruption Volumes

Eruption volumes for the high-silica rhyolites of the Mineral Mountains range from <0.1 to 0.55 km^3 (table 4; fig. 7). The largest is the 851 ka Bailey Ridge obsidian flow. The obsidian flow of Wildhorse Canyon is smaller, with an estimated volume of 0.23 km^3. Individual middle domes have eruptive volumes of approximately 0.1 km^3, for a collective volume of 0.29 km^3. The average eruptive volume of the high domes is 0.23 km^3; the largest are the 483 ka South Twin Flat Mountain and the undated North Twin Flat Mountain, both located in Ranch Canyon. The volume of the pyroclastic deposit, also in Ranch Canyon, was not determined because of limited exposure but was previously estimated to be 0.4 km^3 of material (Nash, 1976). The total eruptive volume for the high-silica rhyolite lavas and domes is about 2.4 km^3, considerably less than the total 15 km^3 estimated by Nash (1976).

Table 4. Estimated eruption volumes of rhyolitic lavas listed in chronological order.

[North Twin Flat Mountain is undated; its position is based on level of dissection relative to other nearby domes. km^3, cubic kilometer]

Sample	Location	Volume (km^3)
	High domes	
17MMST-1	South Twin Flat Mountain	0.33
17MMRCD-1	Ranch Canyon dome	0.07
17MMNTD-1	North Twin Flat Mountain	0.37
17MMND-1	North dome	0.12
17MMBM-2	Bearskin Mountain	0.19
17MMLBM-1	Little Bearskin Mountain	0.27
	Middle domes	
17MMBCCD-1	Big Cedar Cove dome	0.29[a]
17MMWDS-1	South Wildhorse Canyon dome	
17MMWDN-1	North Wildhorse Canyon dome	
	Obsidian flows	
17MMWCF-1	Wildhorse Canyon	0.23
17MMBR-1	Bailey Ridge	0.55

[a]Combined volume for all three middle domes.

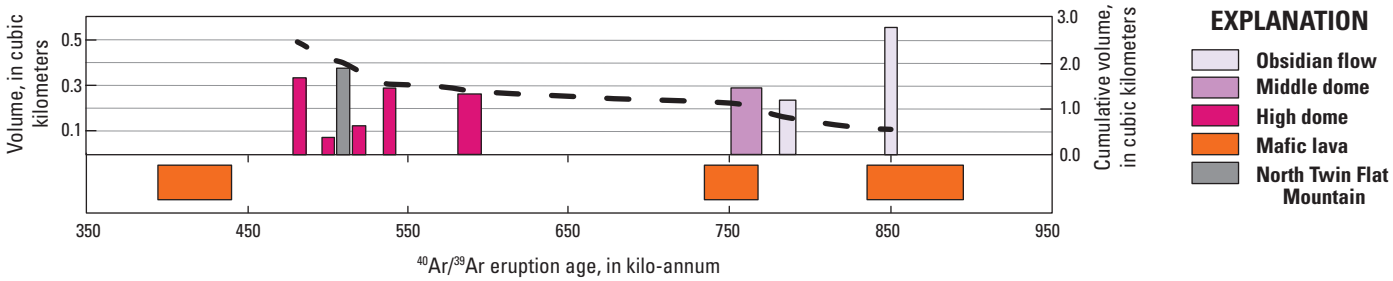

Figure 7. Plot of erupted volumes estimated using QGIS versus $^{40}Ar/^{39}Ar$ eruption ages for high-silica rhyolitic lavas in the Mineral Mountains, southwestern Utah. Note that North Twin Flat Mountain is undated but its volume is included, and its position in the stratigraphy is based on level of dissection (see text for additional details). Cumulative eruption volume through time is shown by the dashed black line. Timing of the mafic to intermediate lavas of the Cove Fort valley as determined in this study are shown below the plot. Width of all bars represents two standard deviation (2σ) uncertainty on $^{40}Ar/^{39}Ar$ ages.

Discussion

Regional Geochemical and Geochronologic Context

Rhyolitic volcanism in the Basin and Range Province extends back to the Oligocene and was largely associated with an ignimbrite flare-up in Nevada. In southwestern Utah, topaz rhyolites erupted between 22 and 18 Ma and again between 13 and 11 Ma (Christiansen and others, 1984, 2007). Located 150 km north of the Mineral Mountains, the Topaz Mountain Rhyolite in the Thomas Range and the rhyolite of the Hogback at Fumarole Butte erupted 7–6 Ma and were followed by the eruption of the rhyolite of Smelter Knolls in the northern Sevier Desert at 3.4 Ma (Peterson and Nash, 1980; Turley and Nash, 1980). Notably, the Thomas Range hosts high-silica topaz rhyolites that are distinctly enriched in fluorine (Christiansen and others, 2007).

The Twin Peaks subfield of the Black Rock Desert volcanic field (2.1–2.7 Ma) is located about 40 km north of the Mineral Mountains and hosts numerous basaltic lavas and at least five distinct rhyolites. The prominent approximately 12 km^3 South Twin Peak dome and Cudahy Mine pumice and obsidian deposits are high-silica rhyolites that do not bear topaz (fig. 8; Crecraft and others, 1981; Johnsen and others, 2014). The youngest rhyolitic volcanism in Utah occurred approximately 55 km to the northeast of the Mineral Mountains. The 400 ka (Nash, 1986) White Mountain dome is an isolated rhyolitic lava characterized by a lithophysae-rich obsidian and a xenolith-bearing stony rhyolite. Most xenoliths are basalts, which neighbor and underlie White Mountain.

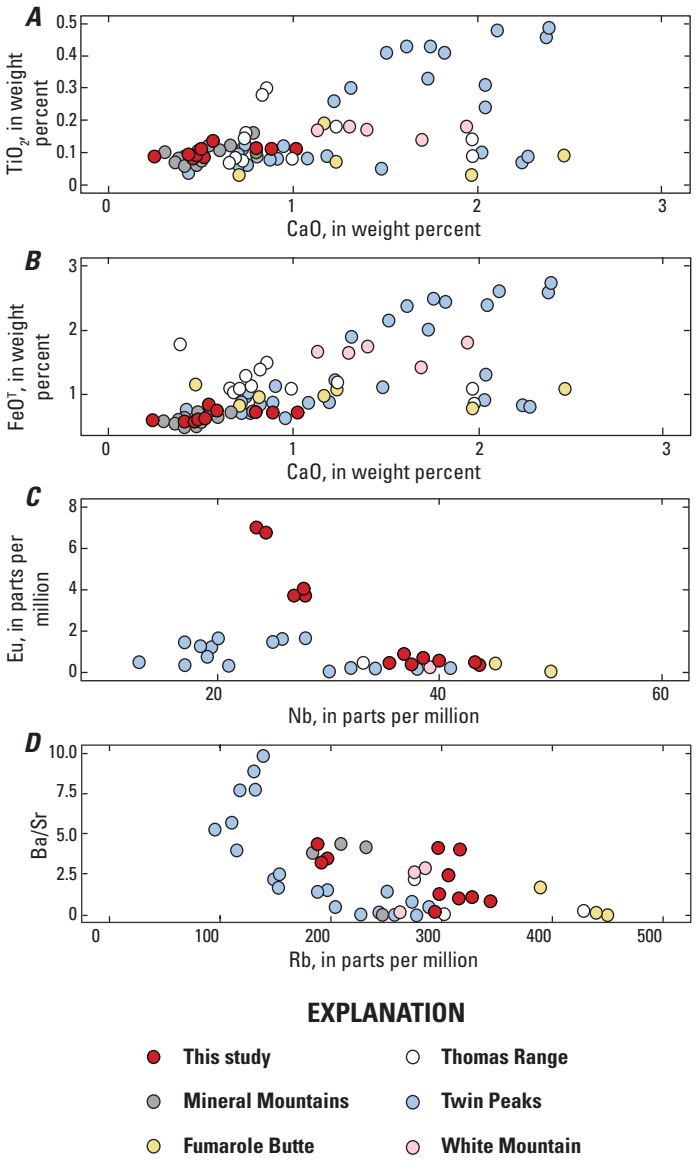

Figure 8. Whole-rock geochemistry of high-silica rhyolites in this study compared to rhyolites of central and southern Utah that erupted less than 10 million years ago. Data from Christiansen and others (1984), Nash (1986), Oviatt (1991), and Johnsen and others (2010). FeO^T, all iron as FeO.

Whereas the Mineral Mountains lavas are temporally correlative to the rhyolite of White Mountain, they are chemically most similar to the 2.7–2.4 Ma high-silica rhyolites (>76 weight percent SiO_2; ≤1 weight percent CaO) of the Twin Peaks volcanic subfield, and in particular, the Cudahy Mine deposits. Johnsen and others (2014) used whole-rock Sr, Nd, and Pb isotopes to show that the range of compositions within the Twin Peaks subfield could be generated through mixing of an enriched mantle type I basalt (Zindler and Hart, 1986) with an evolved rhyolite, which could represent a crustal composition. This model could be applied to the mafic and felsic lavas of the Mineral Mountains and Cove Fort volcanic subfield; however, petrogenetic modeling is not the focus of this study.

Spatial and Temporal Evolution of Volcanism

New $^{40}Ar/^{39}Ar$ geochronology places better temporal constraints on the eruptive history of the Pleistocene rhyolites of the Mineral Mountains and neighboring mafic-intermediate lavas of the Cove Fort valley. Although results are similar to those obtained via the K-Ar technique (Lipman and others, 1978; Best and others, 1980; Nash, 1986), the increased precision on individual eruption ages helps to define eruptive periods and recurrence intervals. Additionally, this work provides the first eruption ages for several of the lavas. Pleistocene rhyolitic volcanism within the Mineral Mountains persisted for ≤400 thousand years (k.y.), and mafic volcanism of the Cove Fort valley may have had a similar duration. Volcanic activity began in the northern part of the range with the eruption of the Black Rock lava flow at 865 ka and the Bailey Ridge obsidian flow at 851 ka (fig. 7 and 9*A*). Uncertainties on these eruption ages allow that the two lavas could have erupted simultaneously on either side of the Mineral Mountains or in sequence separated in time by only a few hundred to thousands of years (fig. 7). Thus, there may be a petrogenetic connection between these two lavas, or another mafic injection beneath Bailey Ridge may have triggered the rhyolitic eruption.

After approximately 65 k.y. of repose, volcanism within the Mineral Mountains migrated south into Wildhorse Canyon with the eruption of the obsidian flow of Wildhorse Canyon (786 ka) and the middle domes (Big Cedar Cove dome, north Wildhorse Canyon dome, and south Wildhorse Canyon dome) at 770–760 ka (fig. 9*B*). Previous workers concluded that the obsidian flows of Bailey Ridge and Wildhorse Canyon were the same age based on the nearly identical whole-rock major and trace element geochemistry and the reversed polarity of both units (Nash, 1986). However, new $^{40}Ar/^{39}Ar$ dating indicates that these two flows are distinct, despite their similar chemistry, and erupted approximately 65 k.y. apart. Although a vent has not been identified, it seems probable that the obsidian flow of Wildhorse Canyon vented from one of the Wildhorse Canyon domes. An eruption age of 786 ka for the Wildhorse Canyon obsidian flow is consistent with field relations that suggest the obsidian dammed the canyon, producing a local basin that subsequently captured the approximately 765 ka Bishop Tuff fallout (Nash, 1976; Andersen and others, 2017). The mineralogical and whole-rock geochemical similarities among the three middle domes may indicate that they are all sourced from the same large magma body. Using feldspar-liquid equilibria and trace element concentrations, Evans and Nash (1978) demonstrated that the more evolved lavas could be produced via fractional crystallization from the magma that produced the obsidian flows. To the east, the intermediate lavas of Cunningham Wash and Crater Knoll erupted around the same time as the eruption of the middle domes (fig. 7), suggesting that the influx of mafic material at this time may have provided the heat needed to generate the rhyolitic melts in the Mineral Mountains (Valentine and others, 2021).

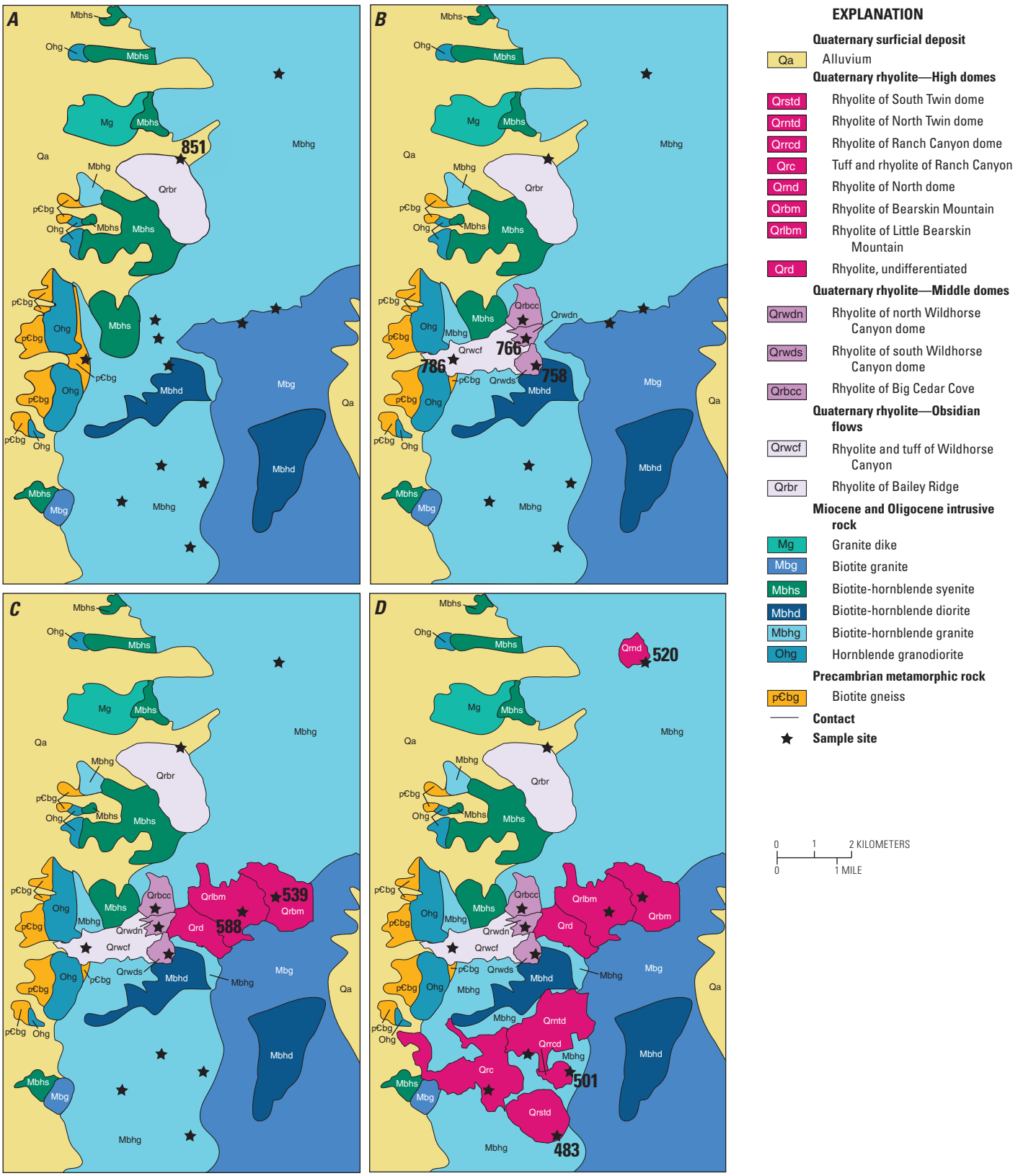

Figure 9. Maps showing the spatial and temporal progression of Pleistocene volcanism within the Mineral Mountains, southwestern Utah. Location is the same as in figure 1*B*. *A* and *B*, Eruption of the obsidian flow of Bailey Ridge at 851 kilo-annum (ka) is followed by the eruption of the obsidian flow of Wildhorse Canyon (786 ka) and middle dome lavas (766–758 ka). *C*, Eruption of the rhyolites of Little Bearskin and Bearskin Mountains (588 and 539 ka, respectively). *D*, Eruption of high dome lavas along the range crest between 520 and 483 ka. Ages are those obtained in this study; stars indicate sample collection sites. Rock types and contacts of granitoids prior to eruptions is inferred. Geology modified from Kirby (2019).

The eruptions of the middle domes were followed by approximately 180 k.y. of inactivity. Volcanism next occurred up-canyon at higher elevations at 588 ka with the eruption of the Little Bearskin Mountain dome, followed by Bearskin Mountain dome at 539 ka (fig. 9*C*). The rhyolites of Little Bearskin and Bearskin Mountains erupted through Miocene granitoids and appear to be structurally controlled by the contact between granitoid rock types (Kirby, 2019). Subsequent volcanism was constrained to higher elevations, producing the high domes of North dome (520 ka), North Twin Flat Mountain (undated), Ranch Canyon dome (501 ka), and South Twin Flat Mountain (483 ka; fig. 9*D*). The high domes are compositionally more evolved than the older eruptions, as indicated by their large negative Eu anomalies (fig. 3), greater concentrations of Rb and Nb, and more varied Ba/Sr ratios (fig. 2). The apparent recurrence interval for these high domes is approximately 20 k.y., and eruptions appear to young toward the south. Overall, the eruptive trend within the mountain range is that less evolved compositions erupted early and closest to the valley floor, whereas progressively more differentiated lavas erupted at higher elevations over time. The temporal, spatial, and compositional trends may be explained through progressive differentiation of a shared magma body, as suggested by Evans and Nash (1978).

Recurrence Intervals within the Mineral Mountains

Recent work by Valentine and others (2021) estimated that Quaternary basaltic monogenetic volcanism of the broader American Southwest has a recurrence interval of <3 k.y.; they further note that eruptions in space and time are intrinsically irregular. However, the recurrence interval for individual Quaternary volcanic fields ranges from 3.6 to 27 k.y. with an average of 15 k.y. (table 5). Whereas the duration of rhyolitic volcanism in the Mineral Mountains is much shorter (<400 k.y.) relative to the basaltic fields of the American Southwest, we calculate a recurrence interval of 33 k.y. (table 5) over the lifetime of the field, from about 850 to 480 ka. If we subdivide the Mineral Mountains rhyolites into two main phases of volcanism, an early approximately 93 k.y. phase consisting of the obsidian flows and middle domes and a later approximately 105 k.y. phase consisting of the high domes (fig. 7), the recurrence interval of the early phase becomes 23 k.y. and the later phase has a recurrence interval of 18 k.y. (table 5), consistent with averages for individual volcanic fields across the region. Although recurrence intervals vary from one volcanic field to another, our work in the Mineral Mountains suggests that basalts and rhyolites erupt in similar long-term patterns on the order of tens of thousands of years.

Although recurrence intervals for recent small-volume silicic eruptions have received less attention from modern high-precision $^{40}Ar/^{39}Ar$ geochronology studies, numerous studies have investigated the timing of pre-, syn-, and post-caldera rhyolitic activity in areas such as Yellowstone Caldera, Valles Caldera, and Long Valley Caldera systems. In the Yellowstone Caldera system, small-volume rhyolites erupted within several thousand years of the 1.3 Ma caldera-forming Mesa Falls Tuff (Rivera and others, 2016; Troch and others, 2017; Stelten and others, 2018). In the Valles Caldera system, frequent eruptions of post-caldera, small-volume rhyolites began immediately after caldera formation and continued for more than 100 k.y. (Nasholds and Zimmerer, 2022). As part of their work, Nasholds and Zimmerer (2022) divided the 34 post-caldera units into 17 eruptive events

Table 5. Recurrence interval estimates for select Quaternary volcanic fields in the American Southwest.

[Only Quaternary volcanoes are included; thus, recurrence intervals are not inferred beyond this period. k.y., thousand years; m.y., million years]

Volcanic field	Duration (m.y.)	Number of Quaternary volcanoes or eruptions	Recurrence interval (k.y.)
Basaltic volcanoes[1]			
Springerville, Arizona	1.800	501	3.6
Pinacate, Sonora, Mexico	1.689	416	4.1
San Francisco, Arizona	2.579	260	10
Uinkaret, Arizona	2.579	213	12
Geronimo-San Bernardino, Arizona	2.320	130	18
Potrillo, New Mexico	2.580	124	21
Southwest Utah	2.553	113	23
Lunar Crater, Nevada	2.545	96	27
Average			15
Rhyolitic eruptions[2]			
Mineral Mountains, Utah (all rhyolites)	0.368	12	33
Mineral Mountains, Utah (early phase)	0.093	5	23
Mineral Mountains, Utah (late phase)	0.105	7	18
Average			20

[1]Data from Valentine and others (2021). Duration calculated using the upper and lower age bounds, if provided, or 2.58 mega-annum (Ma) if the volcanic field included eruptions prior to the Quaternary.

[2]Data from this study.

as either pulses, phases, or episodes. They define single events separated by distinct repose periods as pulses, two or more units with indistinguishable ages as phases, and three or more events that have statistically indistinguishable oldest and youngest ages with no discernable repose period between as eruptive episodes. Using their nomenclature, the rhyolites of the Mineral Mountains are eruptive pulses. Nasholds and Zimmerer (2022) calculate recurrence intervals for the post-caldera eruptions at Valles Caldera according to different groupings of pulses, phases, and events; however, if each of the 34 units is considered an eruptive pulse, like we define the Mineral Mountains eruptions, then the recurrence interval for post-caldera resurgence at Valles Caldera over approximately 100 k.y. is 34.2 k.y.

The Coso volcanic field in California is located at the junction of the western Basin and Range Province and the Sierra Nevada, similar in tectonic setting to the Mineral Mountains and Cove Fort valley. Thirty-eight high-silica (>77 weight percent SiO_2, volatile-free), nearly aphyric rhyolites erupted between 1.04 and 0.079 Ma (Bacon, 1982; Burgess and others, 2021), and 14 basalts erupted contemporaneously (1.08 to 0.039 Ma) to the south of the rhyolite domes and lava flows (Bacon and others, 1980; Bacon, 1982). The estimated volume of erupted rhyolites in the Coso volcanic field is 2.4 km^3 (Lanphere and others, 1975), which is identical to the volume calculated in this study for the Mineral Mountains rhyolites. Bacon and others (1981) divided the rhyolites into seven chemical groups that have distinct eruptive periods separated by as little as 5 k.y. to more than 400 k.y. (Burgess and others, 2021). These would be eruptive phases according to the terminology of Nasholds and Zimmerer (2022). Using a duration of 961 k.y. for rhyolitic activity based on existing obsidian glass K-Ar ages (Bacon, 1982) and zircon ^{238}U–^{230}Th ages (Burgess and others, 2021), the recurrence interval for the 38 rhyolitic eruptions of the Coso volcanic field is approximately 25 k.y. However, as Bacon (1982) noted, eruption intervals may be controlled by the volume of material erupted during the previous eruptive phase; thus, smaller eruptions occur more frequently and larger eruptions less often. Our first-order comparison to both extension and caldera-related, small-volume rhyolites indicates that the frequency of eruptions from small- and large-volume silicic systems may be remarkably similar and warrants further investigation to determine if there is a fundamental control on silicic eruptive recurrence rates.

Magmatic Flux of Small-Volume High-Silica Rhyolites

New high precision $^{40}Ar/^{39}Ar$ dating of the Mineral Mountains rhyolites has allowed us to identify two periods of volcanism. Excluding the 865–417 ka mafic-intermediate lavas of the Cove Fort volcanic subfield, we define the early phase (860–750 ka) as the obsidian flows and middle domes, and the later phase (590–480 ka) as the more chemically evolved high domes. The eruptive flux calculated for each approximately 100-k.y.-long period of felsic activity is approximately 0.01 km^3/k.y., which is greater than the rhyolitic flux in the Coso volcanic field (0.003 km^3/k.y.) but markedly less than the syn-resurgent dome (0.05 km^3/k.y.) or post-caldera (2.66 km^3/k.y.) eruptive fluxes from the Valles Caldera (Nasholds and Zimmerer, 2022).

The amount of nonerupted silicic material is largely unknown in the Mineral Mountains despite the excellent exposures of underlying plutons. In numerous localities globally, it has been suggested that silicic magmas may form a viscous rheologic barrier that may block eruption of subsequent magmas, causing them to stagnate within the crust (for example, Hildreth, 1981; Streck and others, 2015; Galetto and others, 2017; Burgess and others, 2021). It has also been suggested that some small-volume eruptions may occur along the periphery of the rheological barrier or within the barrier in areas of regional extension. Using these models for the Mineral Mountains, the rheological barrier may be the Oligocene to Miocene granitic batholith that underlies the high-silica rhyolites. The granitic plutons may suppress the eruption of basalt, forcing voluminous basalts to erupt in the adjacent Cove Fort valley (that is, along the periphery of the batholith), whereas small-volume rhyolites may be generated through anatectic melting of the granitoids (Nash, 1986) and ascend to the surface via zones of local extension. The rheological barrier may also explain the absence of a basaltic eruption preceding the high domes at approximately 588 ka. Rather than erupting the basalt, the heat may have been transferred to the granitoids to generate the high domes.

This model is similar to others proposed for volcanic fields of the American Southwest that host significant (>30 percent) evolved magmatism—the input of high-flux basalts in the upper crust provides the heat necessary to sustain long-lived mush zones, leading to the construction of polygenetic volcanoes (Cashman and others, 2017). However, volcanic fields in the American Southwest that have minor evolved magmatism may reflect limited storage and diversification to produce monogenetic volcanoes (Valentine and others, 2021). The contemporaneous eruption of basalt and small-volume rhyolite, along with the lack of basalt within the mountain range, indicates that the input of basaltic magma, at least during the first (early) cycle, may have facilitated eruption of the monogenetic rhyolites of the Mineral Mountains and mafic eruptions along the periphery of the rheological barrier in the adjacent volcanic field. A zircon petrochronology study could aid in resolving timescales of magmatic extraction, diversification, and recharge, as well as relations between the host granites and erupted rhyolites.

Conclusions

The Mineral Mountains in southwestern Utah contain some of the State's youngest small-volume, monogenetic rhyolites, which have long been connected to geothermal development in the region. Our new precise $^{40}Ar/^{39}Ar$ eruption chronology shows the spatial and temporal evolution of Pleistocene volcanism within this range. Bimodal volcanism commenced near the north edge of the range and produced the Black Rock lava flow and obsidian

flow of Bailey Ridge. The early phase of rhyolitic volcanism lasted 93 thousand years (k.y.) and included the eruptions of two obsidian flows and three domes at higher elevations. This was followed by a second phase of more evolved rhyolites that erupted laterally along the range crest. We show that these two episodes of volcanism are characterized by an approximately 20 k.y. recurrence interval, similar to that for Quaternary basaltic volcanism in the American Southwest. Overall, the flux rate during each of the two periods of silicic volcanism is approximately 0.01 cubic kilometers per thousand years, which is markedly less than those of other silicic systems in the American Southwest. However, the heat source that generated these magmas still drives an active hydrothermal system, adjoining conductive system, and melts at relatively shallow depths. Finally, this work provides essential data that can be used in future studies to assess timescales of magma generation, chemical differentiation, and eruption.

References Cited

Andersen, N.L., Jicha, B.R., Singer, B.S., and Hildreth, W., 2017, Incremental heating of Bishop Tuff sanidine reveals pre-eruptive radiogenic Ar and rapid remobilization from cold storage: Proceedings of the National Academy of Sciences, v. 114, p. 12407–12412, https://doi.org/10.1073/pnas.1709581114.

Bacon, C.R., 1982, Time-predictable bimodal volcanism in the Coso Range, California: Geology, v. 10, p. 65–69, https://doi.org/10.1130/0091-7613(1982)10<65:tbvitc>2.0.co;2.

Bacon, C.R., Duffield, W.A., and Nakamura, K., 1980, Distribution of Quaternary rhyolite domes of the Coso Range, California—Implications for extent of the geothermal anomaly: Journal of Geophysical Research Solid Earth, v. 85, p. 2425–2433, https://doi.org/10.1029/jb085ib05p02425.

Bacon, C.R., Macdonald, R., Smith, R.L., and Baedecker, P.A., 1981, Pleistocene high-silica rhyolites of the Coso Volcanic Field, Inyo County, California: Journal of Geophysical Research Solid Earth, v. 86, p. 10223–10241, https://doi.org/10.1029/jb086ib11p10223.

Best, M.G., McKee, E.H., and Damon, P.E., 1980, Space-time-composition patterns of late Cenozoic mafic volcanism, southwestern Utah and adjoining areas: American Journal of Science, v. 280, p. 1035–1050, https://doi.org/10.2475/ajs.280.10.1035.

Biek, R.F., Rowley, P.D., Hayden, J.M., Hacker, D.B., Willis, G.C., Hintze, L.F., Anderson, R.E., and Brown, K.D., 2010, Geologic map of the St. George and east part of the Clover Mountains 30′ × 60′ quadrangles, Washington and Iron Counties, Utah: Utah Geologic Survey Map 242DM, scale 1:100,000.

Burgess, S.D., Coble, M.A., and Vazquez, J.A., 2021, Zircon geochronology and geochemistry of Quaternary rhyolite domes of the Coso volcanic field, Inyo County, California: Journal of Volcanology and Geothermal Research, v. 417, article no. 107276, https://doi.org/10.1016/j.jvolgeores.2021.107276.

Cashman, K.V., Sparks, R.S.J., and Blundy, J.D., 2017, Vertically extensive and unstable magmatic systems—A unified view of igneous processes: Science, v. 355, 9 p., https://doi.org/10.1126/science.aag3055.

Chapman, D. S., Blackwell, D.D., Parry, W.T., Sill, W.R., Ward, S.H., and Whelan, J.A., 1978, Regional heat flow and geochemical studies in southwest Utah: University of Utah Department of Geology and Geophysics Final Report, v. 2, under contract no. 14-08-001-G-341, 118 p.

Christiansen, E.H., Bikun, J.V., Sheridan, M.F., and Burt, D.M., 1984, Geochemical evolution of topaz rhyolites from the Thomas Range and Spor Mountain, Utah: American Mineralogist, v. 69, p. 223–236.

Christiansen, E.H., Haapala, I., and Hart, G.L., 2007, Are Cenozoic topaz rhyolites the erupted equivalents of Proterozoic rapakivi granites? Examples from the western United States and Finland: Lithos, v. 97, p. 219–246, https://doi.org/10.1016/j.lithos.2007.01.010.

Coleman, D.S., and Walker, J.D., 1992, Evidence for the generation of juvenile granitic crust during continental extension, Mineral Mountains Batholith, Utah: Journal of Geophysical Research Solid Earth, v. 97, p. 11011–11024, https://doi.org/10.1029/92jb00653.

Coleman, D.S., Walker, J.D. Bartley, J. M., and Hodges, K.V., 2001, Thermochronologic evidence of footwall deformation during extensional core complex development, Mineral Mountains, Utah, *in* The Geologic Transition, High Plateaus to Great Basin—A Symposium and Field Guide: American Association of Petroleum Geologists Pacific Section Guidebook 78, p. 155–168.

Condie, K. C. and Barsky, C. K., 1972, Origin of Quaternary basalts from the Black Rock Desert region, Utah: Geological Society of America Bulletin, v. 83, p. 333–352.

Crecraft, H.R., Nash, W.P., and Evans, S.H., 1981, Late Cenozoic volcanism at Twin Peaks, Utah—Geology and petrology: Journal of Geophysical Research, v. 86, p. 10303–10320.

Evans, S.H., and Nash, W.P., 1978, Quaternary rhyolite from the Mineral Mountains, Utah, U.S.A.: U.S. Department of Energy, prepared by authors under contract no. EY-76-S-07-1601, 59 p.

Ewert, J.W., Diefenbach, A.K., and Ramsey, D.W., 2018, Update to the U.S. Geological Survey National Volcanic Threat Assessment: U.S. Geological Survey Scientific Investigations Report 2018–5140, 40 p., https://doi.org/10.3133/ sir20185140.

Galetto, F., Acocella, V., and Caricchi, L., 2017, Caldera resurgence driven by magma viscosity contrasts: Nature Communications, v. 8, article no. 1750, https://doi.org/10.1038/s41467-017-01632-y.

Hildreth, W., 1981, Gradients in silicic magma chambers—Implications for lithospheric magmatism: Journal of Geophysical Research Solid Earth, v. 86, p. 10153–10192, https://doi.org/10.1029/jb086ib11p10153.

Jicha, B.R., Singer, B.S., and Sobol, P., 2016, Re-evaluation of the ages of $^{40}Ar/^{39}Ar$ sanidine standards and super-eruptions in the western U.S. using a Noblesse multi-collector mass spectrometer: Chemical Geology, v. 431, p. 54–66, https://doi.org/10.1016/j.chemgeo.2016.03.024.

Johnsen, R.L., Smith, E.I., and Biek, R.K., 2010, Subalkaline volcanism in the Black Rock Desert and Markagunt Plateau volcanic fields of south-central Utah, *in* Carney, S.M., Tabet, D.E., and Johnson, C.L., eds., Geology of South-Central Utah, v. 39, p. 109–150.

Johnsen, R., Smith, E., and Walker, D., 2014, The 2.7–2.1 Ma Twin Peaks Caldera—Stratigraphy and petrogenesis, *in* MacLean, J.S., Biek, R.F., and Huntoon, J.E., eds., Geology of Utah's Far South: Utah Geological Association Publication 43, p. 617–638.

Kirby, S.M., 2019, Revised mapping of bedrock geology adjoining the Utah FORGE site, *in* Allis, R., and Moore, J.N., eds., Geothermal Characteristics of the Roosevelt Hot Springs System and Adjacent FORGE EGS Site, Milford, Utah: Utah Geological Survey Miscellaneous Publication 169-A, 6 p., 2 plates, scale 1:24,000, https://doi.org/10.34191/MP-169-A.

Knaack, C., Cornelius, S.B., and Hooper, P R., 1994, ICP-MS method—Trace element analyses of rocks and minerals by ICP-MS: Washington State University GeoAnalytical Laboratory website, accessed May 9, 2024, at https://environment.wsu.edu/facilities/geoanalytical-lab/technical-notes/icp-ms-method.

Lanphere, M.A., Dalrymple, G.B., and Smith, R.L., 1975, K-Ar ages of Pleistocene rhyolitic volcanism in the Coso Range, California: Geology, v. 3, p. 339–341, https://doi.org/10.1130/0091-7613(1975)3<339:kaoprv>2.0.co;2.

Lee, J.-Y., Marti, K., Severinghaus, J.P., Kawamura, K., Yoo, H.-S., Lee, J.B., and Kim, J.S., 2006, A redetermination of the isotopic abundances of atmospheric Ar: Geochimica et Cosmochimica Acta, v. 70, p. 4507–4512, https://doi.org/10.1016/j.gca.2006.06.1563.

Lipman, P.W., Rowley, P.D., Mehnert, H.H., Evans, S.H., Jr., Nash, W.P., and Brown, F.H., 1978, Pleistocene rhyolite of the Mineral Mountains, Utah—Geothermal and archaeological significance: Journal Research of the U.S. Geological Survey, v. 6, p. 133–147.

Min, K., Mundil, R., Renne, P.R., and Ludwig, K.R., 2000, A test for systematic errors in $^{40}Ar/^{39}Ar$ geochronology through comparison with U/Pb analysis of a 1.1-Ga rhyolite: Geochimica et Cosmochimica Acta, v. 64, p. 73–98, https://doi.org/10.1016/s0016-7037(99)00204-5.

Nash, W.P., 1976, Petrology of the Quaternary volcanics of the Roosevelt KGRA and adjoining area: National Science Foundation, prepared by author under contract no. GI-43741, 114 p.

Nash, W.P., 1986, Distribution, lithology and ages of Late Cenozoic volcanism on the eastern margin of the Great Basin, west-central Utah: U.S. Department of Energy, prepared by author under contract no. DEACO780 ID 12079, 82 p.

Nasholds, M.W.M., and Zimmerer, M.J., 2022, High-precision $^{40}Ar/^{39}Ar$ geochronology and volumetric investigation of volcanism and resurgence following eruption of the Tshirege Member, Bandelier Tuff, at the Valles caldera: Journal of Volcanology and Geothermal Research, v. 431, article no. 107624, https://doi.org/10.1016/j.jvolgeores.2022.107624.

Nielson, D.L., Evans, S.H., and Sibbett, B.S., 1986, Magmatic, structural, and hydrothermal evolution of the Mineral Mountains intrusive complex, Utah: Geological Society of America Bulletin, v. 97, p. 765–777, https://doi.org/10.1130/0016-7606(1986)97<765:msaheo>2.0.co;2.

Nielson, D.L., Sibbett, B.S., McKinney, D.B., Hulen, J.B., Moore, J.N., and Samberg, S.M., 1978, Geology of Roosevelt Hot Springs KGRA, Beaver County, Utah: U.S. Department of Energy, prepared by University of Utah Research Institute under contract no. EG-78-C-07-1701, 54 p., https://doi.org/10.2172/5696785.

Oviatt, C.G., 1991, Quaternary geology of the Black Rock Desert, Millard County, Utah: Utah Geological and Mineral Survey Special Studies 73, 23 p., https://doi.org/10.34191/ofr-128.

Peterson, J.B., and Nash, W.P., 1980, Geology and petrology of the Fumarole Butte volcanic complex, Utah, *in* Studies in Late Cenozoic volcanism in west-central Utah: Utah Geological and Mineral Survey Special Studies 52, p. 34–58.

Rivera, T.A., Schmitz, M.D., Jicha, B.R., and Crowley, J.L., 2016, Zircon petrochronology and $^{40}Ar/^{39}Ar$ sanidine dates for the Mesa Falls Tuff—Crystal-scale records of magmatic evolution and the short lifespan of a large Yellowstone magma chamber: Journal of Petrology, v. 57, p. 1677–1704, https://doi.org/10.1093/petrology/egw053.

Rivera, T.A., Storey, M., Schmitz, M.D., and Crowley, J.L., 2013, Age intercalibration of $^{40}Ar/^{39}Ar$ sanidine and chemically distinct U/Pb zircon populations from the Alder Creek Rhyolite Quaternary geochronology standard: Chemical Geology, v. 345, p. 87–98, https://doi.org/10.1016/j.chemgeo.2013.02.021.

Robinson, R., and Iyer, H.M., 1979, Evidence from teleseismic P-wave observations for a low velocity body under the Roosevelt Hot Springs geothermal area, Utah: Geothermal Resources Council Transactions, v. 3, p. 585.

Sibbett, B.S., and Nielson, D.L., 1980, Geology of the central Mineral Mountains Beaver County, Utah: U.S. Department of Energy, prepared by University of Utah Research Institute under contract no. AC07-78ET28392, 54 p.

Smith, I.E.M., and Nemeth, K., 2017, Source to surface model of monogenetic volcanism—A critical review, *in* Nemeth, K., Carrasco-Nuñez, G., Aranda-Gomez, J.J., and Smith, I.E.M., eds., Monogenetic Volcanism: Geological Society of London Special Publications, v. 446, p. 1–28, https://doi.org/10.1144/sp446.14.

Smith, R.L., Bailey, R.A., and Ross, C.S., 1970, Geologic map of the Jemez Mountains, New Mexico: U.S. Geological Survey Miscellaneous Geologic Investigations Map I-571, scale 1:125,000.

Spell, T.L., and Harrison, T.M., 1993, $^{40}Ar/^{39}Ar$ geochronology of post-Valles Caldera rhyolites, Jemez Volcanic Field, New Mexico: Journal of Geophysical Research Solid Earth, v. 98, p. 8031–8051, https://doi.org/10.1029/92jb01786.

Stelten, M.E., Champion, D.E., and Kuntz, M.A., 2018, The timing and origin of pre- and post-caldera volcanism associated with the Mesa Falls Tuff, Yellowstone Plateau volcanic field: Journal of Volcanology and Geothermal Research, v. 350, p. 47–60, https://doi.org/10.1016/j.jvolgeores.2017.12.002.

Streck, M.J., Ferns, M.L., and McIntosh, W., 2015, Large, persistent rhyolitic magma reservoirs above Columbia River Basalt storage sites—The Dinner Creek Tuff Eruptive Center, eastern Oregon: Geosphere, v. 11, p. 226–235, https://doi.org/10.1130/ges01086.1.

Sun, S.-S., and McDonough, W.F., 1989, Chemical and isotopic systematics of oceanic basalts—Implications for mantle composition and processes: Geological Society of London Special Publications, v. 42, p. 313–345, https://doi.org/10.1144/gsl.sp.1989.042.01.19.

Turley, C.H.., and Nash, W.P., 1980, Petrology of late Tertiary and Quaternary volcanism in western Juab and Millard Counties, Utah, *in* Studies in Late Cenozoic volcanism in west-central Utah: Utah Geological and Mineral Survey Special Studies 52, p. 1–33.

Troch, J., Ellis, B.S., Mark, D.F., Bindeman, I.N., Kent, A.J.R., Guillong, M., and Bachmann, O., 2017, Rhyolite generation prior to a Yellowstone super-eruption—Insights from the Island Park–Mount Jackson Rhyolite Series: Journal of Petrology, v. 58, no. 1, p. 29–52, https://doi.org/10.1093/petrology/egw071.

U.S. Geological Survey, 2021, U.S. Geological Survey 3D Elevation Program 1/3 arc-second digital elevation model: U.S. Geological Survey dataset distributed by OpenTopography, accessed October 13, 2023, at https://doi.org/10.5069/G98K778D.

Valentine, G.A., Ort, M.H., and Cortés, J.A., 2021, Quaternary basaltic volcanic fields of the American Southwest: Geosphere, v. 17, p. 2144–2171, https://doi.org/10.1130/ges02405.1.

Ward, S.H., Parry, W.T., Nash, W.P., Sill, W.R., Cook, K.L., Smith, R.B., Chapman, D.S., Brown, F.H., Whelan, J.A., and Bowman, J.R., 1978, A summary of the geology, geochemistry, and geophysics of the Roosevelt Hot Springs thermal area, Utah: Geophysics, v. 43, p. 1515–1542, https://doi.org/10.1190/1.1440912.

Zindler, A., and Hart, S., 1986, Chemical geodynamics: Annual Review of Earth and Planetary Sciences, v. 14, p. 493–571.

Moffett Field Publishing Service Center, California
Approved for publication on August 5, 2024
Edited by Monica Erdman
Layout and design by Cory Hurd

ISSN 2330-7102 (online)
https://doi.org/10.3133/pp1890K